(This is a sample cover image for this issue. The actual cover is not yet available at this time.)

European Journal of Mechanics A/Solids 31 (2012) 163–178

Contents lists available at SciVerse ScienceDirect

European Journal of Mechanics A/Solids

journal homepage: www.elsevier.com/locate/ejmsol

A novel formulation for integrating nonlinear kinematic hardening Drucker-Prager's yield condition

Mohammad Rezaiee-Pajand[a,*], Mehrzad Sharifian[b]

[a] Civil Engineering, Ferdowsi University of Mashhad, Mashhad, Khorasan Razavi 91775-1111, Iran
[b] Structural Engineering, Ferdowsi University of Mashhad, Iran

ARTICLE INFO

Article history:
Received 7 March 2011
Accepted 8 August 2011
Available online 18 August 2011

Keywords:
Plasticity
Numerical integration
Error control
Drucker-Prager
Nonlinear hardening

ABSTRACT

The Drucker-Prager's plasticity model obeying nonlinear kinematic and linear isotropic hardenings is considered. A new integration formulation is suggested that is based on definitions of angles between the strain rate and the shifted stress, and between the shifted stress and back stress in the deviatoric plane. This method will reduce the constitutive relations to five ordinary differential equations (ODEs). For solving this system of ODEs, the embedded pairs and local error estimation schemes along with FSAL property are used. As a result, an integration scheme is developed with automatic error control. The updated stress produced by the proposed numerical scheme is consistent with the yield condition. Finally, a broad set of numerical tests are carried out to investigate the accuracy and efficiency of the suggested technique.

1. Introduction

When the plastic deformations of materials are involved, the nonlinear finite element methods along with the theory of plasticity are commonly used for solving this kind of engineering problems. The accuracy and efficiency of the overall nonlinear finite element analysis are directly associated with the robustness of the stress updating process. The stress updating is carried out by integrating the constitutive equations at each Gauss point. This integration is normally done by a numerical method because the analytical exact integrations for a few plasticity models are merely available.

In the past century, numerous investigations have been done to develop and examine the integration methods. These comprehensive studies are because of the issue importance and for the reason that a variety of the plasticity models and hardening rules are existed. Wilkins (1964) proposed the radial return integration, which the scheme needs a purely elastic predictor and a plastic corrector (return mapping). A closed-form exact solution for the elastic-perfectly plastic von-Mises model was suggested by Krieg and Krieg (1977). Yoder and Whirley (1984) developed an analytical integration for the von-Mises model with a condition of purely kinematic hardening, and a perturbation solution by considering the isotropic hardening effects. Ortiz and Popov (1985) preformed comprehensive studies on the accuracy and stability of the well-known integration schemes, such as the radial return procedure. A family of return mapping schemes for the plane stress elasto-plastic problem was proposed by Simo and Taylor (1986). Loret and Prevost (1986) presented an accurate solution for the Drucker-Prager's criterion along with a linear hardening rule and arbitrary degree of non-associability. In their research, an ordinary differential equation has been derived, which can be integrated by an accurate Runge-Kutta procedure.

For the case of the von-Mises criterion with mixed hardening, Dodds (1987) examined common numerical integrations. Runesson et al. (1988) presented a limited accuracy analysis for constitutive equations for the behavior of metals as well as concrete and soil. Sloan and Booker (1992) showed the Tresca constitutive law may be integrated exactly under plane strain conditions. In their study, a semi-analytical algorithm for Mohr-Coulomb plasticity model was derived. Ristinmaa and Tryding (1993) suggested a unified approach which could include all the earlier exact integration algorithms. Genna and Pandolfi (1994) provided a two-step integration scheme for the Drucker-Prager's yield surface with linear mixed hardening. The return mapping algorithm for a class of cyclic plasticity models was extended by Hopperstad and Remseth (1995). Wie et al. (1996) proposed a consistent algorithm for Prandtl-Reuss elastic-perfectly plastic materials. Their stress updating scheme combines the advantages of the exact solution and the rapid convergence of Newton iteration technique.

* Corresponding author. Tel.: +98 915 313 0340; fax: +98 511 8412912.
E-mail address: mrpajand@yahoo.com (M. Rezaiee-Pajand).

0997-7538/$ – see front matter © 2011 Elsevier Masson SAS. All rights reserved.
doi:10.1016/j.euromechsol.2011.08.004

In the current century, the rate of the development for the integration methods in plasticity has been even increased. As a result, the exponential-based method has been developed based on the internal symmetries of the plasticity models. For the internal symmetries constitutive equations, the plastic consistency condition is satisfied if the numerical solution could consider it (Hong and Liu, 2000, 2001; Liu, 2003, 2004a). In addition to these developments, the schemes based on Euler's integrations have been proposed for the new plasticity models. Sloan et al. (2001) refined effective explicit integrations with automatic error control for the Cam clay family. Wallin and Ristinmaa (2001) reformulated the constitutive equations to a system of ordinary differential equations. In their study, the fifth-order *Dormand-Prince* scheme 5(4) is used for solving this system of ODEs. Moreover, an algorithmic tangent stiffness tensor and its approximate evaluation were derived. A comprehensive investigation on the application of the differential-algebraic equations (DAEs) in nonlinear finite element analysis was performed by Ellsiepen and Hartmann (2001). In this study, the system of DAEs was connected to the Multilevel-Newton method. It is worth mentioning that the system of DAEs is obtained from coupling the mechanical balance laws (which are algebraic equations) and the constitutive equations of the internal variables (which are ordinary differential equations). Kobayashi and Ohno (2002) implemented an integration algorithm based on the backward Euler method for a cyclic plasticity model.

Auricchio and Beirão da Veiga (2003) suggested a non-consistent integration scheme based on an exponential map for the associative von-Mises plasticity with linear hardening. Kobayashi et al. (2003) presented an implicit integration and its consistent tangent modulus in the case of constitutive equations, which depend to time and temperature. Liu (2004b) derived two explicit exponential-based integrations for the elastic-perfectly plastic Drucker-Prager's model. Hartmann (2005) presented remarks on the application of the classical Newton–Raphson algorithm related to the finite element method and compared it with the classical and improved version of the Multilevel-Newton method. Artioli et al. (2005) presented two consistent exponential-based schemes for the von-Mises yield surface with linear mixed hardening. Clausen et al. (2006) developed a return mapping scheme for constitutive relations with multiple yield planes. A second-order explicit exponential scheme for the von-Mises material with linear mixed hardening was extended by Artioli et al. (2006). Rezaiee-Pajand and Nasirai (2007) derived a semi-implicit exponential-based integration with quadratic rate of convergence for the von-Mises plasticity model along with linear mixed hardening. Artioli et al. (2007) suggested a second-order exponential algorithm for the von-Mises plasticity governed by linear isotropic and Armstrong-Frederick's kinematic hardening. Rezaiee-Pajand and Nasirai (2008) proposed 2 second-order semi-implicit stress updating schemes for the elastic-perfectly plastic Drucker-Prager model.

Wallin and Ristinmaa (2008) presented a reduced set of ODEs from the von-Mises isotropic hardening plasticity coupled to damage models. It was demonstrated that an additional set of ODEs for consistent tangent stiffness tensor is needed, which should be solved simultaneously with the reduced set of the former ODEs. Szabó (2009) developed a semi-analytical algorithm for von-Mises plasticity with linear isotropic hardening. Followed by, two semi-analytical integrations in the case of the combined linear isotropic-kinematic hardening von-Mises plasticity were provided by Kossa and Szabó (2009). These solutions correspond with the strain-driven and stress-driven problems, which are developed by using the assumptions of constant strain and stress rates, respectively. Coombs et al. (2010) derived an analytical backward Euler algorithm for the modified Reuleaux model. Rezaiee-Pajand et al. (2010) proposed an exponential-based integration for the von-Mises plasticity with multi-component nonlinear kinematic hardening. Finally, an accurate solution and approximate integrations of the Drucker-Prager's constitutive equations with linear mixed hardening were presented by Rezaiee-Pajand et al. (2011).

In the present study, the Drucker-Prager's constitutive equations governed by linear isotropic and nonlinear kinematic hardenings are considered. A new integration formulation is derived, which is based on introducing the angle between the strain rate and the shifted stress, and the angle between the shifted stress and back stress in the deviatoric plane. The constitutive equations are reduced to five ordinary differential equations (ODEs). The derived differential equations can be solved by ODE integration techniques. The third-order *Bogacki-Shampine* method 3(2) and the fifth-order *Dormand-Prince* scheme 5(4) are used for medium and high accuracies, respectively. These approaches were designed to produce an estimate of the local truncation error for a single Runge–Kutta step. In addition, an extra advantage of these approaches is having FSAL (*First Same As Last*) property. As a result, an effective scheme for integrating the nonlinear constitutive equations will be developed, which can effectively control the errors. A wide range of numerical tests is provided to investigate the accuracy and efficiency of the new integration. These tests include strain load histories, iso-error maps, and computation time.

2. Constitutive equations

In this study, it is assumed that the realm of the deformations is small. The Drucker-Prager's criterion (Drucker and Prager, 1952) with nonlinear kinematic and linear isotropic hardenings is adopted. This yield function is a simple modification of the von-Mises plasticity model that the effect of the hydrostatic pressure on the failure is considered by the inclusion of an additional term as follows:

$$F = \frac{1}{2}\mathbf{s}' : \mathbf{s}' - (\tau_y - \beta p')^2, \quad \tau_y - \beta p' > 0 \tag{1}$$

where, τ_y denotes the yield stress in pure shear, and β is a material parameter related to yielding. The evolution of the yield stress is represented by a linear isotropic hardening. The parameters $\mathbf{s}'$ and p' denote the deviatoric shifted stress and the hydrostatic shifted stress as:

$$\boldsymbol{\sigma}' = \mathbf{s}' + p'\mathbf{i} \text{ with } p' = \frac{1}{3}\mathrm{tr}(\boldsymbol{\sigma}') \tag{2}$$

In this equation, $\mathbf{i}$ represents the second-order identity tensor. Also, 'tr' denotes the trace operator. The shifted stress, $\boldsymbol{\sigma}'$, is defined by the next relation:

$$\boldsymbol{\sigma}' = \boldsymbol{\sigma} - \mathbf{a} \tag{3}$$

Where the total stress and the total back stress were denoted by $\boldsymbol{\sigma}$ and $\mathbf{a}$, respectively. As a usual, the back stress represents the center of the yield surface in the stress space. For convenience, the total strain, ε, is split into the deviatoric strain, $\mathbf{e}$, and the volumetric strain, ε_v, as below:

$$\boldsymbol{\varepsilon} = \mathbf{e} + \frac{1}{3}\varepsilon_{\mathrm{v}}\mathbf{i} \text{ with } \varepsilon_{\mathrm{v}} = \mathrm{tr}(\boldsymbol{\varepsilon}) \tag{4}$$

The additive decomposition of the strain into elastic and plastic parts is used by the following relations:

$$\boldsymbol{\varepsilon} = \boldsymbol{\varepsilon}^{\mathrm{e}} + \boldsymbol{\varepsilon}^{\mathrm{p}} \tag{5}$$

$$\mathbf{e} = \mathbf{e}^{\mathrm{e}} + \mathbf{e}^{p} \tag{6}$$

$$\varepsilon_{\mathrm{v}} = \varepsilon_{\mathrm{v}}^{\mathrm{e}} + \varepsilon_{\mathrm{v}}^{\mathrm{p}} \tag{7}$$

Now, an associative flow rule is adopted to determine the plastic strain rate as:

$$\dot{\boldsymbol{\varepsilon}}^{\mathrm{p}} = \dot{\gamma}\frac{\partial F}{\partial \boldsymbol{\sigma}'} \tag{8}$$

Where, the term $\dot{\gamma}$ is the plastic multiplier. Using Eq. (1), the last relation can be written in below form:

$$\dot{\boldsymbol{\varepsilon}}^{p} = \dot{\gamma}\left[\mathbf{s}' + \frac{2}{3}\beta(\tau_{\mathrm{y}} - \beta p')\mathbf{i}\right] \tag{9}$$

Using the last equation, the rate of the volumetric plastic strain, i.e. $\mathrm{tr}(\dot{\boldsymbol{\varepsilon}}^{\mathrm{p}})$, is easily determined as follows:

$$\dot{\varepsilon}_{\mathrm{v}}^{p} = 2\beta\dot{\gamma}(\tau_{\mathrm{y}} - \beta p') \tag{10}$$

In the present study, a linear isotropic hardening is adopted. This rule can be introduced by the equation:

$$\tau_{\mathrm{y}} = \tau_{\mathrm{y},0} + H_{\mathrm{iso}}\gamma \tag{11}$$

where, $\tau_{\mathrm{y},0}$ denotes the initial yield stress in pure shear, and H_{iso} is the linear isotropic hardening modulus. The kinematic hardening rule presents the translation of the yield surface as a rigid body during plastic yielding. An Armstrong and Frederick's kinematic hardening, which is the most well-known nonlinear kinematic hardening rule (Armstrong and Frederick, 1966), is utilized. A *recall* term (called *dynamic recovery*) in this rule has been defined that incorporates the fading memory effect on the strain path. The subsequent evolution law of the back stress is expressed according to the Armstrong and Frederick rule:

$$\dot{\mathbf{a}} = H_{\mathrm{kin}}\dot{\boldsymbol{\varepsilon}}^{\mathrm{p}} - \dot{\gamma}H_{\mathrm{nl}}\mathbf{a} \tag{12}$$

Where, the constants H_{kin} and H_{nl} are the material parameters. This rule is presented in the deviatoric plane in the below form:

$$\dot{\boldsymbol{\alpha}} = H_{\mathrm{kin}}\dot{\mathbf{e}}^{\mathrm{p}} - \dot{\gamma}H_{\mathrm{nl}}\boldsymbol{\alpha} \tag{13}$$

In the last equation, α signifies the deviatoric part of the back stress, and it can be defined as follows:

$$\boldsymbol{\alpha} = \mathbf{a} - \overline{p}\mathbf{i} \text{ with } \overline{p} = \frac{1}{3}\mathrm{tr}\left(\mathbf{a}\right) \tag{14}$$

Where, $\overline{p}$ is the volumetric part of the back stress. The rate of the shifted stress for isotropic materials is obtained by taking the time derivative of Eq. (3) and using the generalized Hooke's law and Eq. (12). As a result, the following relation will be valid:

$$\dot{\boldsymbol{\sigma}}' = 2G\dot{\boldsymbol{\varepsilon}}^{\mathrm{e}} + \left(K - \frac{2}{3}G\right)\dot{\varepsilon}_{\mathrm{v}}^{\mathrm{e}}\mathbf{i} - H_{\mathrm{kin}}\dot{\boldsymbol{\varepsilon}}^{\mathrm{p}} + \dot{\gamma}H_{\mathrm{nl}}\mathbf{a} \tag{15}$$

In this equation, G and K are the shear and bulk modulus, respectively. The rate of the hydrostatic shifted stress can be achieved by using Eqs. (2) and (15) as:

$$\dot{p}' = K\dot{\varepsilon}_{\mathrm{v}} - \overline{K}\dot{\varepsilon}_{\mathrm{v}}^{\mathrm{p}} + \dot{\gamma}H_{\mathrm{nl}}\overline{p} \tag{16}$$

Where, $\overline{K}$ is expressed as:

$$\overline{K} = K + \frac{1}{3}H_{\mathrm{kin}} \tag{17}$$

Now, the radius of the yield surface in the deviatoric plane, R, is defined by:

$$R = \sqrt{2}(\tau_{\mathrm{y}} - \beta p') \tag{18}$$

Then, substituting Eq. (10) into Eq. (16) and using the last relation yield:

$$\dot{p}' = K\dot{\varepsilon}_{\mathrm{v}} - \sqrt{2}\beta\overline{K}\dot{\gamma}R + \dot{\gamma}H_{\mathrm{nl}}\overline{p} \tag{19}$$

This relationship specifies the governing differential equation of the hydrostatic shifted stress. The rate of the volumetric part of the back stress, $\overline{p}$, can be obtained by using Eqs. (14), (12), (10) and the definition of the radius of the yield surface as:

$$\dot{\overline{p}} = \frac{\sqrt{2}}{3}H_{\mathrm{kin}}\beta\dot{\gamma}R - \dot{\gamma}H_{\mathrm{nl}}\overline{p} \tag{20}$$

Using Eqs. (9) and (10), the rate of the plastic deviatoric strain can be found, which has the below form:

$$\dot{\mathbf{e}}^{p} = \dot{\gamma}\mathbf{s}' \tag{21}$$

The rate of the deviatoric part of the shifted stress, $\dot{\mathbf{s}}'$, can be determined based on the rate of elastic deviatoric strain and the deviatoric back stress by:

$$\dot{\mathbf{s}}' = 2G\dot{\mathbf{e}}^{\mathrm{e}} - \dot{\boldsymbol{\alpha}} \tag{22}$$

Substituting Eqs. (13) and (21) into the last equation leads to the following constitutive equation for the deviatoric shifted stress:

$$\dot{\mathbf{s}}' = 2G\dot{\mathbf{e}} - 2\overline{G}\dot{\gamma}\mathbf{s}' + \dot{\gamma}H_{\mathrm{nl}}\boldsymbol{\alpha} \tag{23}$$

where,

$$2\overline{G} = 2G + H_{\mathrm{kin}} \tag{24}$$

To complete the basic equations, the Kuhn-Tucker loading/unloading conditions are given as follows:

$$\dot{\gamma} \geq 0, \quad F \leq 0, \quad \dot{\gamma}F = 0 \tag{25}$$

According to the last complementary conditions, the state of the material is plastic (or elastoplastic) if $\{\dot{\gamma} > 0 \text{ and } F = 0\}$, and elastic if $\{\dot{\gamma} = 0 \text{ and } F \leq 0\}$. Finally, the plastic multiplier, $\dot{\gamma}$, can be derived by using the consistency condition, i.e. $\dot{\gamma}\dot{F} = 0$ if $F = 0$, during plastic yielding:

$$\dot{\gamma} = \frac{2G\mathbf{s}' : \dot{\mathbf{e}} + \sqrt{2}\beta KR\dot{\varepsilon}_{\mathrm{v}}}{2\left(\overline{G} + \overline{K}\beta^2\right)R^2 + \sqrt{2}(H_{\mathrm{iso}} - \beta H_{\mathrm{nl}}\overline{p})R - H_{\mathrm{nl}}\mathbf{s}' : \boldsymbol{\alpha}} \tag{26}$$

2.1. Remark 1

While yielding in many metals, such as iron-based materials and aluminum, is depended to pressure, the plastic deformation is essentially incompressible (Spitzig and Richmond, 1984). Plastic incompressibility can be considered by means of a non-associative flow rule based on the following plastic potential (Lei and Lissenden, 2007):

$$Q = \frac{1}{2}\mathbf{s}' : \mathbf{s}' \tag{27}$$

The non-associated potential flow has the below form:

$$\dot{\boldsymbol{\varepsilon}}^{\mathrm{p}} = \dot{\mathbf{e}}^{\mathrm{p}} = \dot{\gamma}\frac{\partial Q}{\partial \boldsymbol{\sigma}'} = \dot{\gamma}\mathbf{s}' \tag{28}$$

Therefore, while yielding of material is pressure sensitive, the volume does not change ($\dot{\varepsilon}_{\mathrm{v}}^{\mathrm{p}} = 0$). In this case, the deviatoric part of the back stress is equal to the total back stress, i.e. $\boldsymbol{\alpha} = \mathbf{a}$ and $\overline{p} = 0$. Furthermore, the rate of the hydrostatic shifted stress, p', and the plastic multiplier, $\dot{\gamma}$, can be obtained by:

$$\dot{p}' = K\dot{\varepsilon}_{\mathrm{v}} \tag{29}$$

$$\dot{\gamma} = \frac{2G\mathbf{s}' : \dot{\mathbf{e}} + \sqrt{2}\beta K R \dot{\varepsilon}_v}{2\overline{G}R^2 + \sqrt{2}H_{iso}R - H_{nl}\mathbf{s}' : \boldsymbol{\alpha}} \tag{30}$$

3. A new integration formulation

In order to integrate the constitutive equations, the constant strain rate assumption over the time interval is used. This means that both $\dot{\mathbf{e}}$ and $\dot{\varepsilon}_v$ are kept constant in each time step. It should be added, this assumption has been widely used in both exact and numerical integration methods. Moreover, it is assumed that at beginning time of integrating the stress state becomes plastic, i.e. $\mathbf{s}'$ lies on the yield surface. As a result, based on Eqs. (1) and (18) one can easily write the following relation:

$$R = \|\mathbf{s}'\| \tag{31}$$

The angle (ψ) between the deviatoric shifted stress, $\mathbf{s}'$, and the deviatoric strain rate, $\dot{\mathbf{e}}$, is defined in below form:

$$\mathbf{s}' : \dot{\mathbf{e}} = R\|\dot{\mathbf{e}}\|\cos\ \psi \tag{32}$$

Moreover, an extra angle, ϕ, between the deviatoric shifted stress, $\mathbf{s}'$, and the deviatoric back stress, $\boldsymbol{\alpha}$, is defined as:

$$\mathbf{s}' : \boldsymbol{\alpha} = R\overline{\alpha}\cos\ \phi \tag{33}$$

Where,

$$\overline{\alpha} = \|\boldsymbol{\alpha}\| \tag{34}$$

The definitions of the angles ψ and ϕ are shown in Fig. 1.
Taking the scalar product of Eq. (23) by $\mathbf{s}'$ leads to the relation:

$$\mathbf{s}' : \dot{\mathbf{s}}' = 2G\mathbf{s}' : \dot{\mathbf{e}} - 2\overline{G}\dot{\gamma}\mathbf{s}' : \mathbf{s}' + \dot{\gamma}H_{nl}\mathbf{s}' : \boldsymbol{\alpha} \tag{35}$$

For convenience, one can write the next equalities:

$$\begin{aligned} \mathbf{s}' : \mathbf{s}' &= R^2 \\ \mathbf{s}' : \dot{\mathbf{s}}' &= R\dot{R} \end{aligned} \tag{36}$$

By substituting these relations and Eqs. (32) and (33) into Eq. (35), the following differential equation can be achieved:

$$\dot{R} = 2G\|\dot{\mathbf{e}}\|\cos\ \psi - \dot{\gamma}(2\overline{G}R - H_{nl}\overline{\alpha}\cos\ \phi) \tag{37}$$

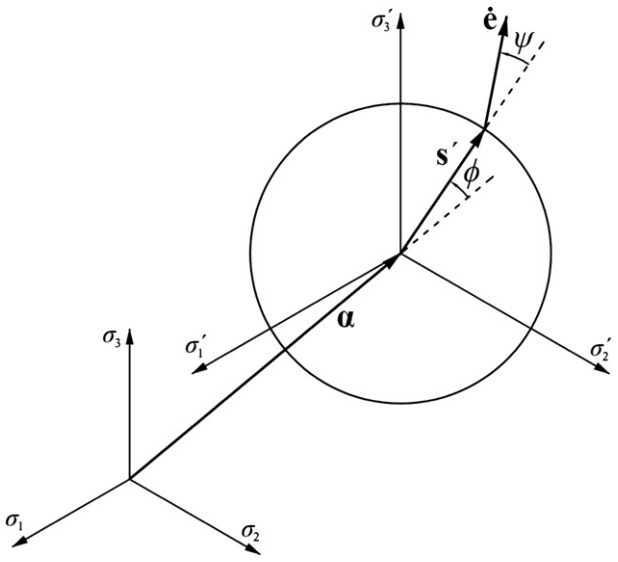

Fig. 1. The definitions of the angles ψ and ϕ.

The last equality is the governing differential equation of the yield surface radius in the deviatoric plane. Substituting Eq. (21) into (13) and taking the scalar product of the result by $\boldsymbol{\alpha}$ give the following expressions:

$$\boldsymbol{\alpha} : \dot{\boldsymbol{\alpha}} = H_{kin}\dot{\gamma}\boldsymbol{\alpha} : \mathbf{s}' - \dot{\gamma}H_{nl}\boldsymbol{\alpha} : \boldsymbol{\alpha} \tag{38}$$

$$\begin{aligned} \boldsymbol{\alpha} : \boldsymbol{\alpha} &= \overline{\alpha}^2 \\ \boldsymbol{\alpha} : \dot{\boldsymbol{\alpha}} &= \overline{\alpha}\dot{\overline{\alpha}} \end{aligned} \tag{39}$$

The evolution equation of $\overline{\alpha}$ is achieved by inserting Eqs. (33) and (39) into Eq. (38) as follows:

$$\dot{\overline{\alpha}} = \dot{\gamma}(H_{kin}R\cos\ \phi - H_{nl}\overline{\alpha}) \tag{40}$$

At this point, it is intended to achieve the evolution equation of ψ. For this purpose, taking the derivative in time of Eq. (32) leads to the next formula:

$$\dot{\mathbf{s}}' : \dot{\mathbf{e}} = \dot{R}\|\dot{\mathbf{e}}\|\cos\ \psi - R\|\dot{\mathbf{e}}\|\dot{\psi}\sin\ \psi \tag{41}$$

Then, taking the scalar product of Eq. (23) by $\dot{\mathbf{e}}$ and using the definition of the angles ψ and ϕ yield the below result:

$$\dot{\mathbf{s}}' : \dot{\mathbf{e}} = 2G\|\dot{\mathbf{e}}\|^2 - 2\overline{G}\dot{\gamma}R\|\dot{\mathbf{e}}\|\cos\ \psi + \dot{\gamma}H_{nl}\overline{\alpha}\|\dot{\mathbf{e}}\|\cos\ (\psi + \phi) \tag{42}$$

By comparing Eqs. (41) and (42) the following relationship will be in hand:

$$\dot{R}\cos\ \psi - R\dot{\psi}\sin\ \psi = 2G\|\dot{\mathbf{e}}\| - 2\overline{G}\dot{\gamma}R\cos\ \psi + \dot{\gamma}H_{nl}\overline{\alpha}\cos\ (\psi + \phi) \tag{43}$$

Now, substituting $\dot{R}$ of Eq. (37) into Eq. (43) and rearranging terms lead to the subsequent rate equation:

$$\dot{\psi} = \frac{1}{R}(\dot{\gamma}H_{nl}\overline{\alpha}\sin\ \phi - 2G\|\dot{\mathbf{e}}\|\sin\ \psi) \tag{44}$$

The rate of the angle ψ obeys the last differential equation. In order to find a rate equation of the angle ϕ, first, taking the scalar product of the deviatoric back stress $\boldsymbol{\alpha}$ by the deviatoric strain rate $\dot{\mathbf{e}}$ is written as:

$$\boldsymbol{\alpha} : \dot{\mathbf{e}} = \overline{\alpha}\|\dot{\mathbf{e}}\|\cos\ (\psi + \phi) \tag{45}$$

Then, taking the derivative in time of this equation gives:

$$\dot{\boldsymbol{\alpha}} : \dot{\mathbf{e}} = \dot{\overline{\alpha}}\|\dot{\mathbf{e}}\|\cos\ (\psi + \phi) - \overline{\alpha}\|\dot{\mathbf{e}}\|\left(\dot{\psi} + \dot{\phi}\right)\sin\ (\psi + \phi) \tag{46}$$

After that, taking the scalar product of Eq. (13) by $\dot{\mathbf{e}}$ and applying Eqs. (21), (32) and (45) will achieve the next relation:

$$\dot{\boldsymbol{\alpha}} : \dot{\mathbf{e}} = H_{kin}\dot{\gamma}R\|\dot{\mathbf{e}}\|\cos\ \psi - \dot{\gamma}H_{nl}\overline{\alpha}\|\dot{\mathbf{e}}\|\cos\ (\psi + \phi) \tag{47}$$

Now, comparing Eqs. (46) and (47), applying Eqs. (40) and (44), and simplifying the results the following differential equation can be obtained:

$$\dot{\phi} = -\frac{1}{\overline{\alpha}}H_{kin}\dot{\gamma}R\sin\ \phi - \frac{1}{R}(\dot{\gamma}H_{nl}\overline{\alpha}\sin\ \phi - 2G\|\dot{\mathbf{e}}\|\sin\ \psi) \tag{48}$$

It is observed that in differential Eqs. (37), (40), (44) and (48) the plastic multiplier, $\dot{\gamma}$, has been appeared. This parameter is a function of the variables R, $\overline{\alpha}$, ψ, ϕ and $\overline{p}$. Therefore, substituting Eqs. (32) and (33) into Eq. (26) can determine a relation for the plastic multiplier, as:

$$\dot{\gamma} = \frac{2GR\|\dot{\mathbf{e}}\|\cos\ \psi + \sqrt{2}\beta K R \dot{\varepsilon}_v}{2\left(\overline{G} + \overline{K}\beta^2\right)R^2 + \sqrt{2}(H_{iso} - \beta H_{nl}\overline{p})R - H_{nl}R\overline{\alpha}\cos\ \phi} \tag{49}$$

Note that the rate of the variable $\overline{p}$ was given by Eq. (20). At this stage, two 5-dimensional vectors are defined as:

$$\boldsymbol{Y} = \begin{Bmatrix} y_1 \\ y_2 \\ y_3 \\ y_4 \\ y_5 \end{Bmatrix} = \begin{Bmatrix} R \\ \overline{\alpha} \\ \psi \\ \phi \\ \overline{p} \end{Bmatrix} \tag{50}$$

and,

$$\boldsymbol{F} = \begin{Bmatrix} f_1 \\ f_2 \\ f_3 \\ f_4 \\ f_5 \end{Bmatrix} = \begin{Bmatrix} 2G\|\dot{\mathbf{e}}\|\cos\ y_3 - \dot{\gamma}(2\overline{G}y_1 - H_{nl}y_2\cos\ y_4) \\ \dot{\gamma}(H_{kin}y_1\cos\ y_4 - H_{nl}y_2) \\ \frac{1}{y_1}(\dot{\gamma}H_{nl}y_2\sin\ y_4 - 2G\|\dot{\mathbf{e}}\|\sin\ y_3) \\ -\frac{1}{y_2}H_{kin}\dot{\gamma}y_1\sin\ y_4 - \frac{1}{y_1}(\dot{\gamma}H_{nl}y_2\sin\ y_4 - 2G\|\dot{\mathbf{e}}\|\sin\ y_3) \\ \dot{\gamma}\left(\frac{\sqrt{2}}{3}H_{kin}\beta y_1 - H_{nl}y_5\right) \end{Bmatrix} \tag{51}$$

Finally, the ordinary differential Eqs. (37), (40), (44), (48) and (20) can be rewritten by the following compact form:

$$\dot{\boldsymbol{Y}} = \boldsymbol{F}(t, y_1, y_2, y_3, y_4, y_5) = \boldsymbol{F}(t, \boldsymbol{Y}) \tag{52}$$

Since there is no analytical solution for this system of ordinary differential equations (ODEs), it can be solved by a numerical integration technique. One type of the most important ODE integrations is the explicit Runge-Kutta families. Two of these strategies for integrating the system of ODEs (52) will be explained in next section. Now, it is intended to integrate the constitutive equations over the time interval $[t_0, t_1]$. The initial conditions for solving the system of ODEs (52) are defined as follows:

$$\boldsymbol{Y}_0 = \begin{Bmatrix} R_0 \\ \overline{\alpha}_0 \\ \psi_0 \\ \phi_0 \\ \overline{p}_0 \end{Bmatrix} \tag{53}$$

Then, solving the system of differential Eq. (52) by an ODE integration technique results in the vector $\boldsymbol{Y}_1$ at time $t = t_1$. Consequently, the deviatoric shifted stress at the end of time step $\mathbf{s}'_1 = \mathbf{s}'(t = t_1)$ can be assumed as a linear combination of $\mathbf{s}'_0 = \mathbf{s}'(t = t_0)$ and $\Delta\mathbf{s}'^{TR}$ in the following form:

$$\mathbf{s}'_1 = \xi\mathbf{s}'_0 + \zeta\Delta\mathbf{s}'^{TR} \tag{54}$$

Where, $\Delta\mathbf{s}'^{TR}$ is an increment of the trial stress, i.e.

$$\Delta\mathbf{s}'^{TR} = 2G\dot{\mathbf{e}}(t_1 - t_0) = 2G\dot{\mathbf{e}}\Delta t \tag{55}$$

The scalar parameters ξ and ζ have the subsequent expressions:

$$\begin{aligned} \xi &= \frac{R_1\sin\psi_1}{R_0\sin\psi_0} \\ \zeta &= \frac{R_1\sin(\psi_0 - \psi_1)}{\|\Delta\mathbf{s}'^{TR}\|\sin\ \psi_0} \end{aligned} \tag{56}$$

It is worth mentioning that the last parameters can be obtained by the relations:

$$\begin{cases} (\xi\mathbf{s}'_0 + \zeta\Delta\mathbf{s}'^{TR}) : \Delta\mathbf{s}'^{TR} = R_1\|\Delta\mathbf{s}'^{TR}\|\cos\ \psi_1 \\ (\xi\mathbf{s}'_0 + \zeta\Delta\mathbf{s}'^{TR}) : \mathbf{s}'_1 = R_1^2 \end{cases} \tag{57}$$

According to the last equations, the suggested integration formulation automatically satisfies the condition of consistency with the yield surface. Also, the deviatoric back stress at time $t = t_1$, i.e. $\boldsymbol{\alpha}_1$, can be achieved by a linear combination of the tensors $\boldsymbol{\alpha}_0$ and $\Delta\mathbf{s}'^{TR}$ as follows:

$$\boldsymbol{\alpha}_1 = \overline{\xi}\boldsymbol{\alpha}_0 + \overline{\zeta}\Delta\mathbf{s}'^{\ TR} \tag{58}$$

Where, the parameters $\overline{\xi}$ and $\overline{\zeta}$ are given by:

$$\begin{aligned} \overline{\xi} &= \frac{\overline{\alpha}_1\sin\ (\psi_1 + \phi_1)}{\overline{\alpha}_0\sin\ (\psi_0 + \phi_0)} \\ \overline{\zeta} &= \frac{\overline{\alpha}_1\sin\ (\psi_0 + \phi_0 - \psi_1 - \phi_1)}{\|\Delta\mathbf{s}'^{TR}\|\sin\ (\psi_0 + \phi_0)} \end{aligned} \tag{59}$$

3.1. Remark 2

If $\psi_0 = 0$ or π, the loading is proportional, and ψ remains equal to zero or π throughout the load step and Eq. (54) will change to the subsequent relation:

$$\mathbf{s}'_1 = \frac{R_1}{R_0}\mathbf{s}'_0 \tag{60}$$

3.2. Remark 3

If $\psi_0 + \phi_0 = 0$ or π, then, $\psi + \phi$ remains equal to zero or π throughout the load step, and Eq. (58) will be formed as:

$$\boldsymbol{\alpha}_1 = \frac{\overline{\alpha}_1}{\overline{\alpha}_0}\boldsymbol{\alpha}_0 \tag{61}$$

4. ODE integrations with error control and FSAL property

In order to integrate the system of ODEs (52), two following methods are used in this study: the third-order *Bogacki-Shampine method 3(2)* (Bogacki and Shampine, 1989) for medium accuracy and the fifth-order *Dormand-Prince method 5(4)* (Dormand and Prince, 1980) for high accuracy. These techniques have the *FSAL* property, and these can estimate the local error to implement adaptive step size. It is worth mentioning that a particularly interesting special class of explicit Runge-Kutta methods, which is used in most modern codes, has the coefficients with FSAL property (so-called *First Same As Last* property). For the ODE integration with this property, the last stage of one integration step is evaluated at the same as the first stage of the next integration step. Furthermore, the adaptive tactics are designed to produce an estimate of the local truncation error of a single Runge-Kutta step. It should be mentioned, the Runge-Kutta methods have already used by the researchers for integrating the constitutive equations and their reduced form (e.g. Sloan and Booker, 1992; Sloan et al., 2001; Wallin and Ristinmaa, 2001, 2008).

4.1. Bogacki-Shampine method 3(2)

The Bogacki-Shampine strategy 3(2) (BSh32) is a Runge-Kutta technique of the third-order with four stages having FSAL

property. Therefore, this approach approximately uses three functions in each step. Moreover, the method has an embedded second-order technique, which can be used to implement adaptive step size. In order to integrate, a time step, $\Delta t = t_{n+1} - t_n$, is considered. Also, it is assumed that $\boldsymbol{Y}_n$ denotes the value of $\boldsymbol{Y}$ at the time $t = t_n$. Now, using the Bogacki-Shampine tactic, the system of ODEs (52) can be integrated numerically to find $\boldsymbol{Y}_{n+1}$ at $t = t_{n+1}$ by the following equations:

$$\boldsymbol{Y}_{n+1} = \boldsymbol{Y}_n + \Delta t\left(\frac{2}{9}\boldsymbol{k}_1 + \frac{1}{3}\boldsymbol{k}_2 + \frac{4}{9}\boldsymbol{k}_3\right) \tag{62}$$

$$\overline{\boldsymbol{Y}}_{n+1} = \boldsymbol{Y}_n + \Delta t\left(\frac{7}{24}\boldsymbol{k}_1 + \frac{1}{4}\boldsymbol{k}_2 + \frac{1}{3}\boldsymbol{k}_3 + \frac{1}{8}\boldsymbol{k}_4\right) \tag{63}$$

All the vectors appeared in these equations are calculated as:

$$\begin{aligned}
\boldsymbol{k}_1 &= \boldsymbol{F}(t_n, \boldsymbol{Y}_n)\\
\boldsymbol{k}_2 &= \boldsymbol{F}\left(t_n + \frac{1}{2}\Delta t, \boldsymbol{Y}_n + \frac{1}{2}\Delta t\boldsymbol{k}_1\right)\\
\boldsymbol{k}_3 &= \boldsymbol{F}\left(t_n + \frac{3}{4}\Delta t, \boldsymbol{Y}_n + \frac{3}{4}\Delta t\boldsymbol{k}_2\right)\\
\boldsymbol{k}_4 &= \boldsymbol{F}(t_{n+1}, \boldsymbol{Y}_{n+1})
\end{aligned} \tag{64}$$

Where, $\overline{\boldsymbol{Y}}_{n+1}$ and $\boldsymbol{Y}_{n+1}$ are the second-order and third-order approximations to the exact solution, respectively. Therefore, the difference between these vectors can be used to implement adaptive step size. Since the method has the FSAL property, the value $\boldsymbol{k}_4$ in one integration step equals the value $\boldsymbol{k}_1$ in the next step and effectively three function evaluations are computed in each time step. The local truncation error in $\boldsymbol{Y}_{n+1}$ can be computed by:

$$\boldsymbol{E}_{n+1} = \boldsymbol{Y}_{n+1} - \overline{\boldsymbol{Y}}_{n+1} = \Delta t\left(-\frac{5}{72}\boldsymbol{k}_1 + \frac{1}{12}\boldsymbol{k}_2 + \frac{1}{9}\boldsymbol{k}_3 - \frac{1}{8}\boldsymbol{k}_4\right) \tag{65}$$

Utilizing Eq. (65), the scalar measure of the relative local error can be defined by the next equality:

$$E = \max\left\{\frac{|E_1|}{|y_1|}, \frac{|E_2|}{|y_2|}, \frac{|E_3|}{|y_3|}, \frac{|E_4|}{|y_4|}, \frac{|E_5|}{|y_5|}\right\}_{n+1} \tag{66}$$

In this relation, E_i (where, $i = 1, 2, \ldots, 5$) is the i th component of the vector $\boldsymbol{E}_{n+1}$. Now, the relative local error can be utilized for determining the size of the next step. The following equation is widely used in the integral step size controller (Shampine and Watts, 1976):

$$\Delta t_{n+1} = 0.9\Delta t_n\left(\frac{Tol}{E}\right)^{\frac{1}{3}} \tag{67}$$

Where, Δt_{n+1} and Tol denote the size of the next time step and the maximum allowable local error, respectively.

4.2. Dormand-Prince method 5(4)

The Dormand-Prince method 5(4) (DP54) is a member of the embedded Runge-Kutta family in the fifth-order with a FSAL scheme. This procedure has seven stages, but it effectively uses only six function evaluations per step. Moreover, it can estimate the local error to implement the adaptive step size. Once again, it is assumed that $\boldsymbol{Y}_n$ and Δt are the value of vector $\boldsymbol{Y}$ at the time t_n and the size of the time step, respectively. In order to integrate the system of ODEs (52) one step of the Dormand-Prince method is given by the expressions:

$$\boldsymbol{Y}_{n+1} = \boldsymbol{Y}_n + \Delta t\left(\frac{35}{384}\boldsymbol{k}_1 + \frac{500}{1113}\boldsymbol{k}_3 + \frac{125}{192}\boldsymbol{k}_4 - \frac{2187}{6784}\boldsymbol{k}_5 + \frac{11}{84}\boldsymbol{k}_6\right) \tag{68}$$

$$\overline{\boldsymbol{Y}}_{n+1} = \boldsymbol{Y}_n + \Delta t\left(\frac{5179}{57600}\boldsymbol{k}_1 + \frac{7571}{16695}\boldsymbol{k}_3 + \frac{393}{640}\boldsymbol{k}_4 - \frac{92097}{339200}\boldsymbol{k}_5 + \frac{187}{2100}\boldsymbol{k}_6 + \frac{1}{40}\boldsymbol{k}_7\right) \tag{69}$$

and,

$$\begin{aligned}
\boldsymbol{k}_1 &= \boldsymbol{F}(t_n, \boldsymbol{Y}_n)\\
\boldsymbol{k}_2 &= \boldsymbol{F}\left(t_n + \frac{1}{5}\Delta t, \boldsymbol{Y}_n + \frac{1}{5}\Delta t\boldsymbol{k}_1\right)\\
\boldsymbol{k}_3 &= \boldsymbol{F}\left(t_n + \frac{3}{10}\Delta t, \boldsymbol{Y}_n + \frac{3}{40}\Delta t\boldsymbol{k}_1 + \frac{9}{40}\Delta t\boldsymbol{k}_2\right)\\
\boldsymbol{k}_4 &= \boldsymbol{F}\left(t_n + \frac{4}{5}\Delta t, \boldsymbol{Y}_n + \frac{44}{45}\Delta t\boldsymbol{k}_1 - \frac{56}{15}\Delta t\boldsymbol{k}_2 + \frac{32}{9}\Delta t\boldsymbol{k}_3\right)\\
\boldsymbol{k}_5 &= \boldsymbol{F}\left(t_n + \frac{8}{9}\Delta t, \boldsymbol{Y}_n + \frac{19372}{6561}\Delta t\boldsymbol{k}_1 - \frac{25360}{2187}\Delta t\boldsymbol{k}_2 + \frac{64448}{6561}\Delta t\boldsymbol{k}_3 - \frac{212}{729}\Delta t\boldsymbol{k}_4\right)\\
\boldsymbol{k}_6 &= \boldsymbol{F}\left(t_{n+1}, \boldsymbol{Y}_n + \frac{9017}{3168}\Delta t\boldsymbol{k}_1 - \frac{355}{33}\Delta t\boldsymbol{k}_2 + \frac{46732}{5247}\Delta t\boldsymbol{k}_3 + \frac{49}{176}\Delta t\boldsymbol{k}_4 - \frac{5103}{18656}\Delta t\boldsymbol{k}_5\right)\\
\boldsymbol{k}_7 &= \boldsymbol{F}(t_{n+1}, \boldsymbol{Y}_{n+1})
\end{aligned} \tag{70}$$

Where, $\overline{\boldsymbol{Y}}_{n+1}$ and $\boldsymbol{Y}_{n+1}$ represent the fourth-order and fifth-order accurate solution, respectively. An error estimator can be formed by subtracting $\boldsymbol{Y}_{n+1}$ from $\overline{\boldsymbol{Y}}_{n+1}$ as:

$$\boldsymbol{E}_{n+1} = \Delta t\left(\frac{71}{57600}\boldsymbol{k}_1 - \frac{71}{16695}\boldsymbol{k}_3 + \frac{71}{1920}\boldsymbol{k}_4 - \frac{17253}{339200}\boldsymbol{k}_5 + \frac{22}{525}\boldsymbol{k}_6 - \frac{1}{40}\boldsymbol{k}_7\right) \tag{71}$$

The scalar measure of the relative local error can be computed by Eq. (66). In order to determine the size of the next time step, the following equation can be used (Shampine and Watts, 1976):

$$\Delta t_{n+1} = 0.9\Delta t_n\left(\frac{Tol}{E}\right)^{\frac{1}{5}} \tag{72}$$

5. Stress updating schemes with automatic error control

For updating the material state, it is assumed that the strain history is a rectilinear path, such that $\dot{\boldsymbol{\varepsilon}}$ is constant during each time step. This is denoted by $\dot{\boldsymbol{\varepsilon}}_n$ at a discrete time $t = t_n$. The constitutive variables at the time t_n, i.e. $\boldsymbol{\varepsilon}_n$, $\boldsymbol{\sigma}_n$, $\mathbf{a}_n$ and γ_n are all known, and the updated strain $\boldsymbol{\varepsilon}_{n+1}$ is also given at the time t_{n+1}. The proposed numerical scheme must integrate the constitutive variables over the time increment to update the material state. In order to integrate, a strain increment, i.e. $\Delta\boldsymbol{\varepsilon} = \Delta t\dot{\boldsymbol{\varepsilon}} = \boldsymbol{\varepsilon}_{n+1} - \boldsymbol{\varepsilon}_n$, is applied and it is decomposed into deviatoric $\Delta\mathbf{e}$ and volumetric $\Delta\boldsymbol{\varepsilon}_v$ parts. Then, a trial solution for the elastic phase at the end of the time step, i.e. t_{n+1}, is calculated as:

$$\begin{aligned}
\mathbf{s}'^{\mathrm{TR}}_{n+1} &= \mathbf{s}'_n + 2G\Delta\mathbf{e}\\
p'^{\mathrm{TR}}_{n+1} &= p'_n + K\Delta\varepsilon_v\\
\boldsymbol{\alpha}^{\mathrm{TR}}_{n+1} &= \boldsymbol{\alpha}_n\\
\overline{p}^{\mathrm{TR}}_{n+1} &= \overline{p}_n\\
\tau^{\mathrm{TR}}_{y,n+1} &= \tau_{y,n}
\end{aligned} \tag{73}$$

The trial values are admissible, if the following condition is satisfied:

$$\|\mathbf{s}'^{\mathrm{TR}}_{n+1}\|^2 \le 2\left(\tau^{\mathrm{TR}}_{y,n+1} - \beta p'^{\mathrm{TR}}_{n+1}\right)^2 \tag{74}$$

Therefore, the time step is elastic and the variables at the time t_{n+1} are taken as the trial values. If Eq. (74) is not fulfilled, the time step can be divided into an elastic part followed by a plastic part. A scalar parameter $\alpha \in [0,\ 1)$ is introduced, as $\alpha\Delta t$ and $(1-\alpha)\Delta t$ give the elastic part and plastic part of the time step, respectively. This scalar parameter can be computed by:

$$\alpha = \frac{\sqrt{B^2 - 4AC} - B}{2A} \tag{75}$$

where, the scalars A, B and C are given as:

$$\begin{aligned} A &= \|2G\Delta\mathbf{e}\|^2 - 2(\beta K\Delta\varepsilon_{\mathrm{v}})^2 \\ B &= 4G\Delta\mathbf{e} : \mathbf{s}'_n + 4\beta K(\tau_{y,n} - \beta p'_n)\Delta\varepsilon_{\mathrm{v}} \\ C &= \|\mathbf{s}'_n\|^2 - 2(\tau_{y,n} - \beta p'_n)^2 \end{aligned} \tag{76}$$

It should be noted that the parameter α was computed by considering the exact yield condition, i.e. $F = 0$. When the exact condition is replaced by the approximate one $|F| \le tol_F$, which tol_F denotes a small positive tolerance, the algorithm presented by Sloan et al. (2001) can be used for obtaining α. In the following, using this parameter (α), the deviatoric and volumetric components of the shifted stress at the time $t_{n+\alpha}$ can be calculated as follows:

$$\begin{aligned} \mathbf{s}'_{n+\alpha} &= \mathbf{s}'_n + 2G\alpha\Delta\mathbf{e} \\ p'_{n+\alpha} &= p'_n + K\alpha\Delta\varepsilon_{\mathrm{v}} \end{aligned} \tag{77}$$

At this stage, $\mathbf{s}'_{n+\alpha}$ has been lied on the yield surface. To find the updated stress and constitutive quantities at the end of the elastoplastic part of the load step, the system of ODEs (52) should be numerically integrated over the time interval $t = t_{n+\alpha}$ to $t = t_{n+1}$. The initial condition for the system of ODEs at the time $t_{n+\alpha}$ is $\mathbf{Y}_{n+\alpha} = \{R_{n+\alpha},\ \overline{\alpha}_n,\ \psi_{n+\alpha},\ \phi_{n+\alpha},\ \overline{p}_{n+\alpha}\}^T$. Since it is intended to control the error, schemes along with sub-steps should be selected. One way to control accuracy in the solution of an initial value problem is to solve the problem twice by using step sizes Δt and $\Delta t/2$ and then compare the results at the end of the larger step size. But, this approach needs a large amount of calculations for the smaller step size. Also, if it is determined that the obtained results are not admissible, the solution must be repeated. The ODE integration methods mentioned in Section 4 are the ways to resolve this trouble. Generally, each time step may consist of several sub-steps, and the relative local error of each sub-step should be computed to determine the size of the next sub-step based on the maximum allowable local error, *Tol* (for example, see Eq. (67)). In fact, this approach permits the size of each sub-step $\Delta t^j = t^{j+1} - t^j$ (superscript j is a counter for the number of sub-steps) to be varied throughout the interval $t = t_{n+\alpha}$ to $t = t_{n+1}$, i.e. $0 < \Delta t^j \le (1-\alpha)\Delta t_n$.

In each sub-step, the system of ODEs (52) is integrated with the initial condition $\mathbf{Y}^j_{n+\alpha}$ and applying Δt^j into Eqs. (62) and (63) for the BSh32 method, or in the case of the DP54 tactic, Eqs. (68) and (69) are used. After that, the relative local error is computed by Eq. (66). If the relative local error E^j is not greater than the specified error tolerance *Tol*, the present sub-step is admissible, and the size of the next sub-step is given by Eq. (67) for the BSh32 (or Eq. (72) for the DP54 method). But, if the relative error is greater than the specified error tolerance, the present solution is not admissible, and the size of the sub-step must be decreased. One way for computing a smaller sub-step size is using an extrapolation by Eq. (67) for the BSh32 (or Eq. (72) for the DP54). This approach has been used by Sloan et al. (2001) for selecting a smaller sub-step in the case of the sub-step has failed. The integration process is finished when the sum of the sub-steps becomes equal to $(1-\alpha)\Delta t_n$, i.e. $\sum \Delta t^j = (1-\alpha)\Delta t_n$. Finally, using the vector $\mathbf{Y}_{n+1} = \{R_{n+1},\ \overline{\alpha}_{n+1},\ \psi_{n+1},\ \phi_{n+1},\ \overline{p}_{n+1}\}^T$ computed by an ODE method, the following constitutive quantities can be updated:

$$\begin{aligned} \mathbf{s}'_{n+1} &= \xi_n \mathbf{s}'_{n+\alpha} + \zeta_n \Delta\mathbf{s}'^{\mathrm{TR}} \\ \boldsymbol{\alpha}_{n+1} &= \overline{\xi}_n \boldsymbol{\alpha}_{n+\alpha} + \overline{\zeta}_n \Delta\mathbf{s}'^{\mathrm{TR}} \end{aligned} \tag{78}$$

Where, $\Delta\mathbf{s}'^{\mathrm{TR}} = 2G(1-\alpha)\Delta\mathbf{e}$ and the scalar parameters are:

$$\begin{aligned} \xi_n &= \frac{R_{n+1}\sin\ \psi_{n+1}}{R_n \sin\ \psi_{n+\alpha}} \\ \zeta_n &= \frac{R_{n+1}\sin\ (\psi_{n+\alpha} - \psi_{n+1})}{\|\Delta s'^{\mathrm{TR}}\|\sin\ \psi_{n+\alpha}} \end{aligned} \tag{79}$$

Furthermore, the parameters $\overline{\xi}_n$ and $\overline{\zeta}_n$ are given by:

$$\begin{aligned} \overline{\xi}_n &= \frac{\overline{\alpha}_{n+1}\sin\ (\psi_{n+1} + \phi_{\ n+1})}{\overline{\alpha}_{n+\alpha}\sin\ (\psi_{n+\alpha} + \phi_{\ n+\alpha})} \\ \overline{\zeta}_n &= \frac{\overline{\alpha}_{n+1}\sin\ (\psi_{n+\alpha} + \phi_{\ n+\alpha} - \psi_{n+1} - \phi_{\ n+1})}{\|\Delta s'^{\mathrm{TR}}\|\sin\ (\psi_{n+\alpha} + \phi_{\ n+\alpha})} \end{aligned} \tag{80}$$

In order to update the hydrostatic stress, first by using the Eqs. (19) and (20), the following equation is held:

$$\dot{p}' = K\dot{\varepsilon}_{\mathrm{v}} - \sqrt{2}K\beta\dot{\gamma}R - \dot{\overline{p}} \tag{81}$$

Now, Eq. (81) is directly integrated as:

$$p'_{n+1} - p'_{n+\alpha} = \int_{t_{n+\alpha}}^{t_{n+1}} \left(K\dot{\varepsilon}_{\mathrm{v}} - \sqrt{2}K\beta\dot{\gamma}R - \dot{\overline{p}}\right)\mathrm{d}t \tag{82}$$

Then, using Eq. (21) and simplifying the result, the subsequent relationships can be easily obtained:

$$p'_{n+1} - p'_{n+\alpha} = K\int_{t_{n+\alpha}}^{t_{n+1}} \dot{\varepsilon}_v \mathrm{d}t - \sqrt{2}\beta K \int_{t_{n+\alpha}}^{t_{n+1}} \|\dot{\mathbf{e}}^{\mathrm{p}}\|\mathrm{d}t - \int_{t_{n+\alpha}}^{t_{n+1}} \dot{\overline{p}}\mathrm{d}t \tag{83}$$

$$p'_{n+1} = K(1-\alpha)\Delta\varepsilon_{\mathrm{v}} - \sqrt{2}\beta K\|\Delta\mathbf{e}^{\mathrm{p}}\| - \overline{p}_{n+1} + \overline{p}_n + p'_{n+\alpha} \tag{84}$$

Where, $\Delta\mathbf{e}^p$ is obtained by using the basic relation for $\mathbf{s}'_{n+1}$, i.e.

$$\mathbf{s}'_{n+1} = \mathbf{s}_{n+1} - \boldsymbol{\alpha}_{n+1} = \mathbf{s}_n + 2G(\Delta\mathbf{e} - \Delta\mathbf{e}^{\mathrm{p}}) - \boldsymbol{\alpha}_{n+1} \tag{85}$$

Manipulating the above equation, the below equality can be achieved:

$$\Delta\mathbf{e}^p = \frac{1}{2G}(\mathbf{s}_n + 2G\Delta\mathbf{e} - \mathbf{s}'_{n+1} - \boldsymbol{\alpha}_{n+1}) \tag{86}$$

Finally, the yield stress at the time t_{n+1} can be computed by using the definition of the yield surface radius in the deviatoric plane, i.e. Eq. (18). The new stress updating scheme is summarized in a flow chart which is shown in Fig. 2.

5.1. Remark 4

The direction of both angles ψ and ϕ, must be the same because the angle between the back stress and the strain rate is computed by summing the angles ψ and ϕ. Therefore, the angles ψ and ϕ at the time $t = t_{n+\alpha}$ can be computed from the below relationships:

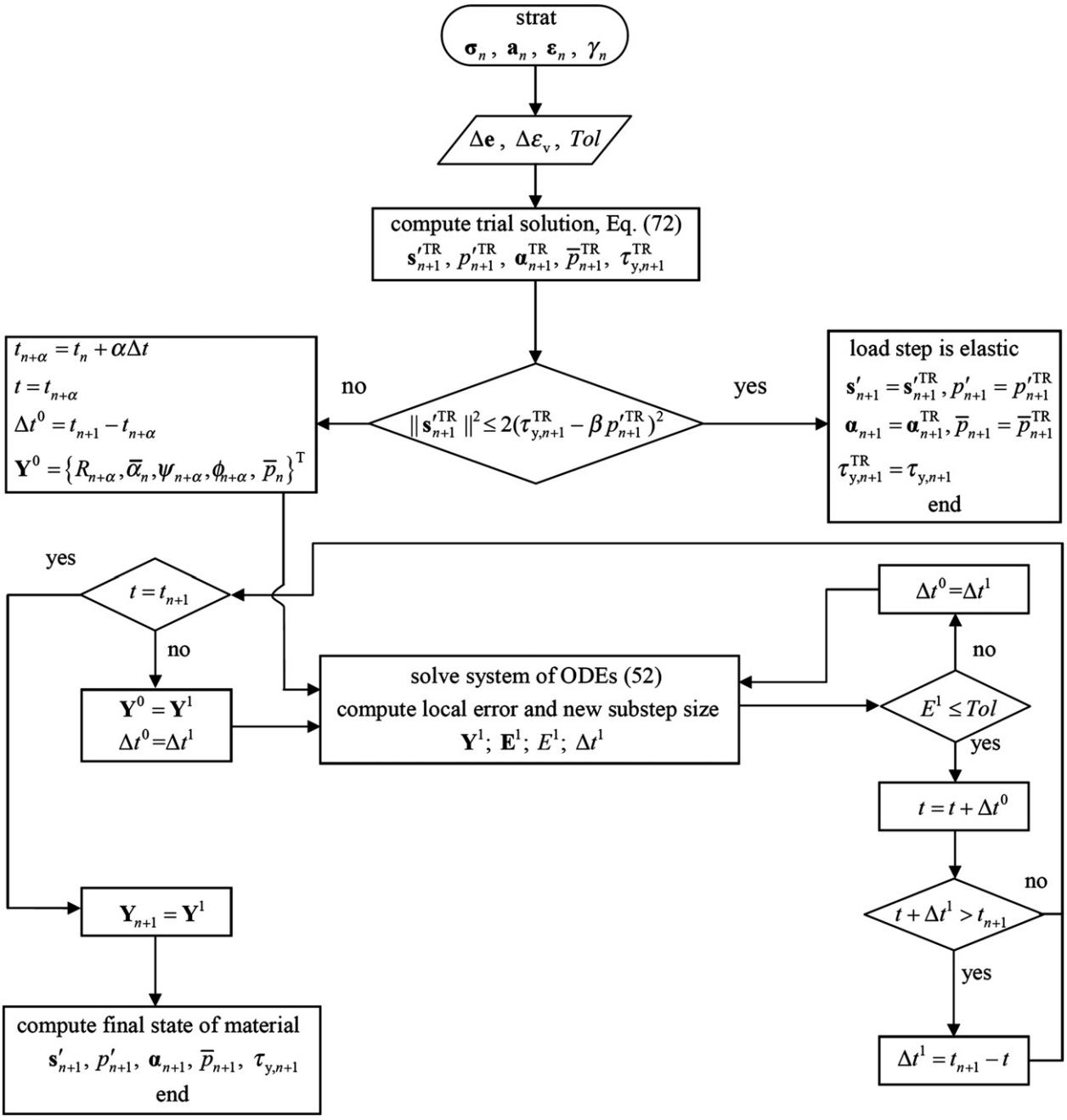

Fig. 2. Flow chart for suggested stress updating scheme.

$$\psi_{n+\alpha} = \cos^{-1}\left(\frac{\mathbf{s}'_{n+\alpha} : \Delta\mathbf{e}}{R_n \|\Delta\mathbf{e}\|}\right) \tag{87}$$

$$\phi_{n+\alpha} = \begin{cases} \kappa_{n+\alpha} & \text{if } \cos(\chi_{n+\alpha}) = \cos(\psi_{n+\alpha} + \kappa_{n+\alpha}) \\ -\kappa_{n+\alpha} & \text{if } \cos(\chi_{n+\alpha}) \neq \cos(\psi_{n+\alpha} + \kappa_{n+\alpha}) \end{cases} \tag{88}$$

Where,

$$\begin{aligned} \kappa_{n+\alpha} &= \cos^{-1}\left(\frac{\mathbf{s}'_{n+\alpha} : \boldsymbol{\alpha}_n}{R_{n+\alpha}\bar{\alpha}_n}\right) \\ \chi_{n+\alpha} &= \cos^{-1}\left(\frac{\boldsymbol{\alpha}_n : \Delta\mathbf{e}}{\bar{\alpha}_n \|\Delta\mathbf{e}\|}\right) \end{aligned} \tag{89}$$

5.2. Remark 5

A consistent tangent stiffness tensor is required to preserve the quadratic asymptotic convergence for the Newton iteration method in a nonlinear finite element analysis. Consistency implies that the stresses obtained by the tangent stiffness tensor must be matched the stresses updated by the integration scheme to the first order. Computing the tangent operator is briefly presented in the following. The discrete consistent tangent operator is derived by linearizing the stress updating method as:

$$\frac{d\boldsymbol{\sigma}_{n+1}}{d\boldsymbol{\varepsilon}_{n+1}} = \left(\frac{d\mathbf{s}'_{n+1}}{d\mathbf{e}_{n+1}} + \frac{d\boldsymbol{\alpha}_{n+1}}{d\mathbf{e}_{n+1}}\right)\mathbb{I}_{dev} + \left(\frac{dp'_{n+1}}{d\varepsilon_{v,n+1}} + \frac{d\bar{p}_{n+1}}{d\varepsilon_{v,n+1}}\right)\mathbf{i}\otimes\mathbf{i} \tag{90}$$

$$\mathbb{I}_{dev} = \mathbb{I} - \frac{1}{3}\mathbf{i}\otimes\mathbf{i} \tag{91}$$

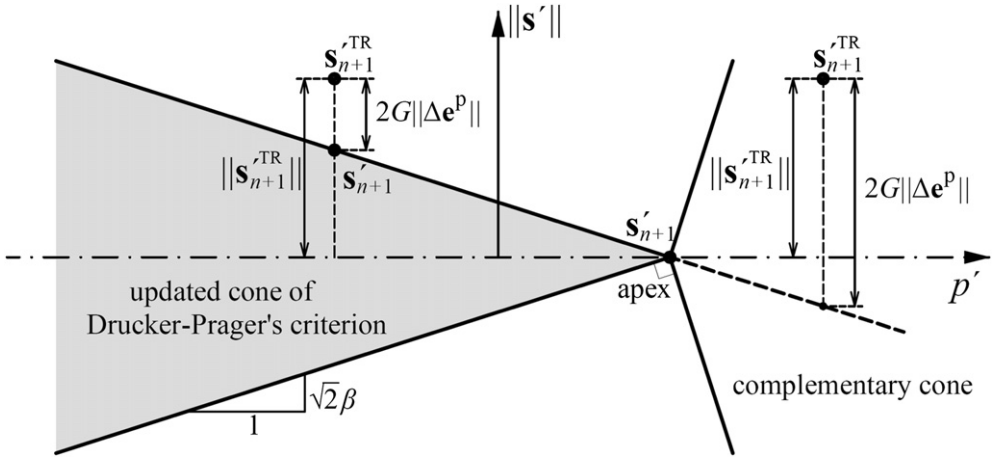

Fig. 3. Choosing the appropriate integration.

Where, $\mathbb{I}$ denotes the fourth-order identity tensor. To compute the derivatives of the tensors appeared in Eq. (90), a derivative of $\boldsymbol{Y}_{n+1}$, i.e. $\boldsymbol{G}_{n+1} = (d\boldsymbol{Y}/d\varepsilon)_{n+1}$ is needed. Taking the time derivative of $\boldsymbol{G}$, the following evolution equation may be in hand:

$$\frac{\mathrm{d}\boldsymbol{G}}{\mathrm{d}t} = \frac{\mathrm{d}\boldsymbol{F}}{\mathrm{d}\boldsymbol{Y}}\frac{\mathrm{d}\boldsymbol{Y}}{\mathrm{d}\boldsymbol{\varepsilon}} \tag{92}$$

At this stage, solving the above system of ODEs simultaneously with the system of ODEs (52) gives the consistent tangent operator and constitutive variables. Both the system of ODEs (52) and (92) can be presented as:

$$\begin{bmatrix}\dot{\boldsymbol{Y}}\\ \dot{\boldsymbol{G}}\end{bmatrix} = \begin{bmatrix}\boldsymbol{F}\\ \dfrac{\mathrm{d}\boldsymbol{F}}{\mathrm{d}\boldsymbol{Y}}\boldsymbol{G}\end{bmatrix} \tag{93}$$

It should be noted, this technique has been already used by Wallin and Ristinmaa (2008) for integrating the damage evolution laws.

6. Treatment of apex

It should be noted that there is a singularity point associated with the apex of the Drucker-Prager's cone. In fact, if the trial stress is situated inside the complementary cone, the stress updated must be located at the apex, i.e. $\mathbf{s}'_{n+1} = 0$ and $R_{n+1} = 0$. If not, updating the material state is the same as the formulation presented earlier (Fig. 3). At the apex, by following the typical methodology, the increment of the plastic multiplier, λ, for a fully plastic load step can be calculated from the next condition:

$$R_{n+1} = \sqrt{2}(\tau_{y,n+1} - \beta p'_{n+1}) = 0 \tag{94}$$

Utilizing the last equation and Eqs. (11) and (19) and adopting an approximate explicit manner, the subsequent plastic multiplier can be obtained:

$$\lambda = \frac{\sqrt{2}\beta K\Delta\varepsilon_v - R_n}{\sqrt{2}H_{iso} - \sqrt{2}\beta H_{nl}\overline{p}_n + 2\beta^2\overline{K}R_n} \tag{95}$$

Now, the other parameters can be updated as:

$$\begin{aligned}
\Delta\mathbf{e}^p &= \lambda\mathbf{s}'_n\\
\boldsymbol{\alpha}_{n+1} &= \boldsymbol{\alpha}_n + H_{kin}\Delta\mathbf{e}^p - \lambda H_{nl}\boldsymbol{\alpha}_n\\
\overline{p}_{n+1} &= \overline{p}_n + \frac{\sqrt{2}}{3}\lambda\beta H_{kin}R_n - \lambda H_{nl}\overline{p}_n\\
\tau_{y,n+1} &= \tau_{y,n} + \lambda H_{iso}\\
p'_{n+1} &= \frac{1}{\beta}\tau_{y,n+1}
\end{aligned} \tag{96}$$

As a result, for integrating the constitutive equations the following algorithm can be tracked. First, the updated state of material is assumed to be on the smooth portion of the cone. In other words, integration is done based on the scheme was presented in Section 5. Subsequently, the below condition is verified:

$$\|\mathbf{s}'^{TR}_{n+1}\| \geq 2G\|\Delta\mathbf{e}^p\| \tag{97}$$

If the last condition is fulfilled, the updated material state is acceptable and is located on the smooth portion. Otherwise, the trial stress is positioned inside the complementary cone, and the updated stress point must be at the apex of the cone. Also, other constitutive variables can be determined by Eqs. (95) and (96). This algorithm is typically used for integrating the Drucker-Prager's constitutive equations (see, for example, References: de Souza Neto et al., 2008; Rezaiee-Pajand et al., 2011).

7. Numerical tests

In order to investigate the accuracy and efficiency of the new integration formulation, a broad set of numerical tests is provided in this section. The assessments are classified in three categories. In the first one, two strain load histories are adopted and the relative error of the stress and back stress output are computed by the new scheme. The robustness of the suggested method is verified by plotting the iso-error maps in the second categories. To show the

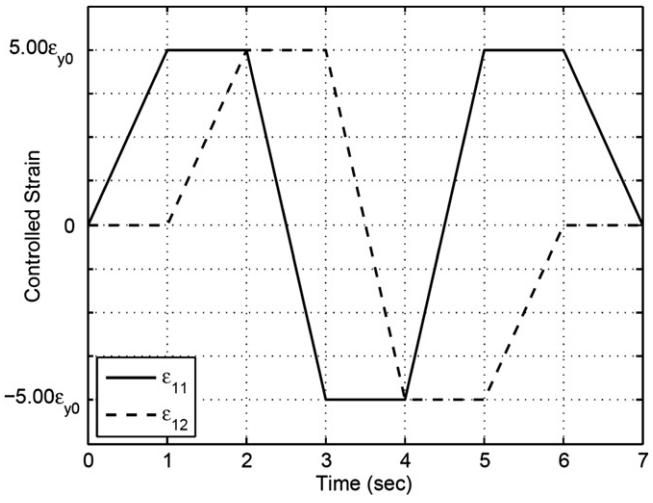

Fig. 4. Strain load history 1.

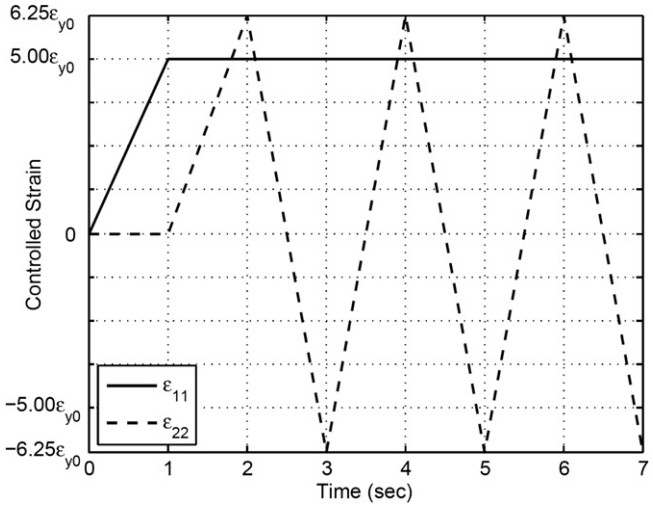

Fig. 5. Strain load history 2.

efficiency and performance of the proposed integration technique, computation time for the new strategy, the forward Euler and the backward Euler methods will be tested and compared. In all numerical examples, the general material properties are adopted as follows (Lei and Lissenden, 2007):

$$E = 1.02 \times 10^5 \text{ MPa};\ \nu = 0.325;\ \tau_{y0} = 156 \text{ MPa};\ \beta = 0.055$$

Moreover, the mechanical properties for the hardening rules are given below:

$$H_{kin} = 24600 \text{ MPa};\ H_{nl} = 118;\ H_{iso} = 500 \text{ MPa}^2$$

Since the suggested integration is based on the definitions of the angles between the quantities, this technique is called *Angles' method*. To make the text self-sufficient, the backward and forward Euler integrations will be briefly presented in Appendices A and B, respectively.

7.1. Strain load histories

Two biaxial non-proportional strain load histories are adopted. In these histories, the strain components are varied proportionally

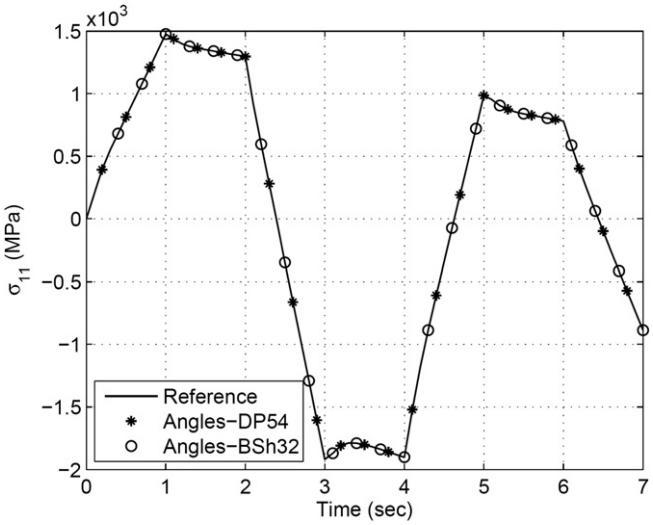

Fig. 6. The history of updated stress component σ_{11} for strain history 1.

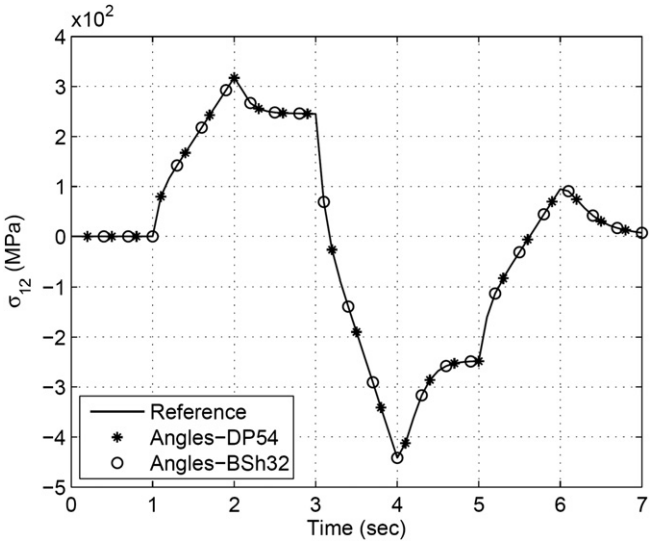

Fig. 7. The history of updated stress component σ_{12} for strain history 1.

to $\varepsilon_{y0} = \sqrt{3}\,(\tau_{y,0}/E)$ while all the other strain components are equal to zero. The strain load history 1 and 2 are given in Figs. 4 and 5, respectively. The strain paths have considered linear to eliminate the discretization errors. First, to verify the correctness of the new integration results, i.e. the Angles' method, the updated stress history associated with the strain history 1 is computed by the backward Euler scheme with a fine time step ($\Delta t = 10^{-5}$ sec) as a 'reference solution' because of lacking the exact solution of the investigated problem. Afterward, using the Angles' integration along with the DP54 and the BSh32 (*Angles-DP54* and *Angles-BSh32*), the stress histories are updated with $\Delta t = 0.1$ sec and $Tol = 10^{-4}$. The histories of two updated stress components σ_{11} and σ_{12} obtained by the new method, and the 'reference' one are plotted in Figs. 6 and 7.

In the next stage, it is intended to assess the accuracy of the new scheme pertaining to the specified error tolerance, *Tol*. To fulfill this aim, three error tolerances $Tol = 10^{-2}$, 10^{-3} and 10^{-4} are considered, and the updated stress is achieved by the Angles' approach and using the BSh32 (Angles-BSh32). To present the

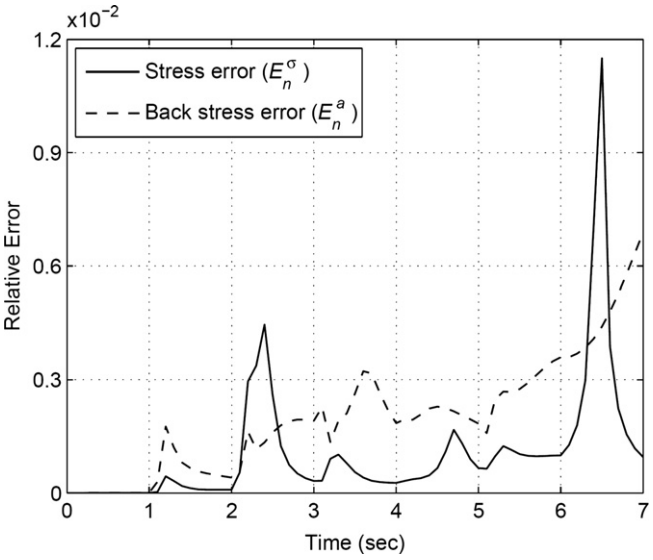

Fig. 8. Stress and back stress relative errors for history 1 by Angles-BSh32 and $Tol = 10^{-2}$.

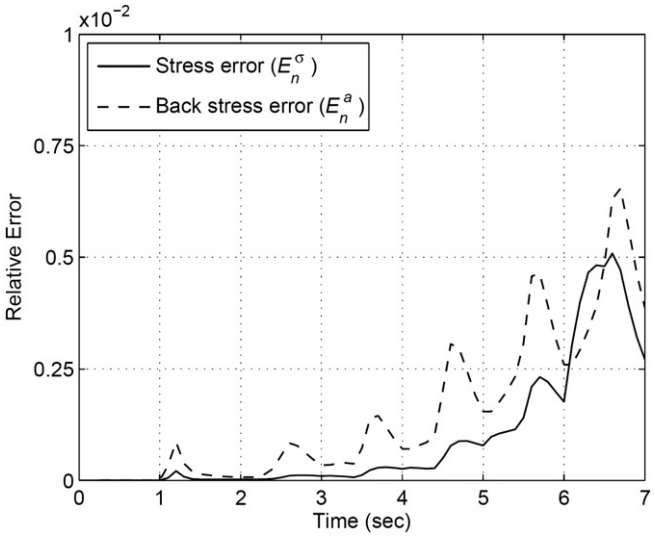

Fig. 9. Stress and back stress relative errors for history 2 by Angles-BSh32 and $Tol = 10^{-2}$.

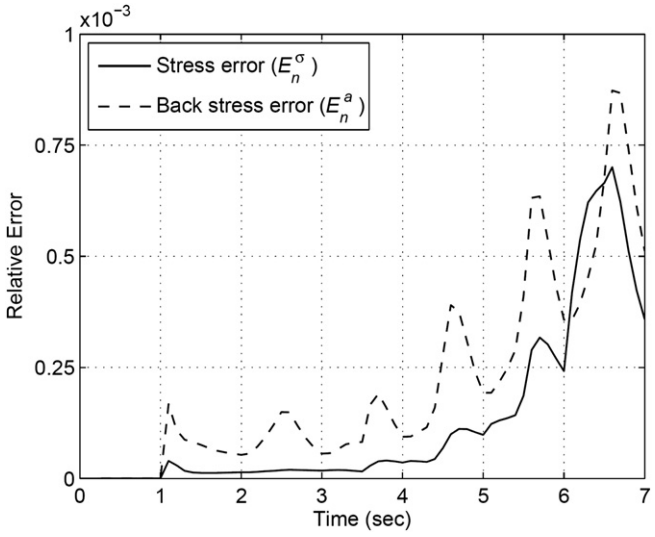

Fig. 11. Stress and back stress relative errors for history 2 by Angles-BSh32 and $Tol = 10^{-3}$.

solution results, the stress and back stress relative errors are calculated by the following equations:

$$E_n^{\sigma} = \frac{\|\boldsymbol{\sigma}_n - \boldsymbol{\sigma}_n^{\mathrm{E}}\|}{\|\boldsymbol{\sigma}_n^{\mathrm{E}}\|} \tag{98}$$

$$E_n^{\mathrm{a}} = \frac{\|\mathbf{a}_n - \mathbf{a}_n^{\mathrm{E}}\|}{\|\mathbf{a}_n^{\mathrm{E}}\|} \tag{99}$$

Where, $\boldsymbol{\sigma}_n$ and $\mathbf{a}_n$ denote stress and back stress, respectively, computed by the Angles-BSh32 at the time t_n. Also, $\boldsymbol{\sigma}_n^{\mathrm{E}}$ and $\mathbf{a}_n^{\mathrm{E}}$ are the stress and back stress, which are updated by the Angles-DP54 with a time step $\Delta t = 0.1$ sec and a stringent error tolerance of $Tol = 10^{-10}$. These are assumed as the 'exact solutions'.

Figs. 8 and 9 show the relative error of the stress and back stress with $Tol = 10^{-2}$ for strain histories 1 and 2, respectively. Furthermore, the relative errors of stresses for two specified error tolerances of 10^{-3} and 10^{-4} are presented in Figs. 10 to 13. As it can be seen in these figures, the errors of the computed stresses are around the specified tolerance error, *Tol*, because the errors are not directly controlled for the stress, $\boldsymbol{\sigma}$, and back stress, $\boldsymbol{\alpha}$, in the Angles' method. In fact, the integration process is performed based on the scalar parameters $\{R, \bar{\alpha}, \psi, \phi, \bar{p}\}$, and the errors are calculated based on these parameters in computation of the stress updating. Therefore, the errors might be slightly more than the specified error tolerance.

7.2. Iso-error maps

It is desired to examine the accuracy and robustness of the new formulation based on the size of the load step and an error tolerance. Therefore, the iso-error maps are utilized as a strong tool for this purpose. The iso-error maps have been successfully used by Krieg and Krieg (1977), Ortiz and Popov (1985), Ortiz and Simo (1896), Loret and Prevost (1986), Genna and Pandolfi (1994), Simo and Hughes (1998), Artioli et al. (2006, 2007), de Souza Neto et al. (2008), Rezaiee-Pajand and Nasirai (2008) and Wallin and Ristinmaa (2008).

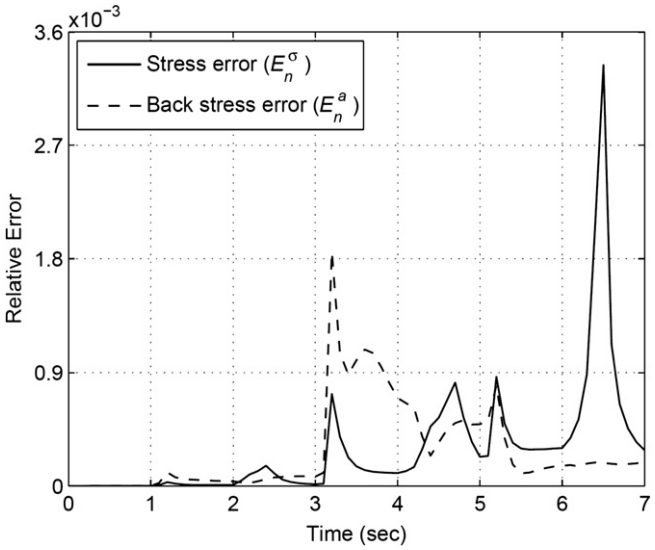

Fig. 10. Stress and back stress relative errors for history 1 by Angles-BSh32 and $Tol = 10^{-3}$.

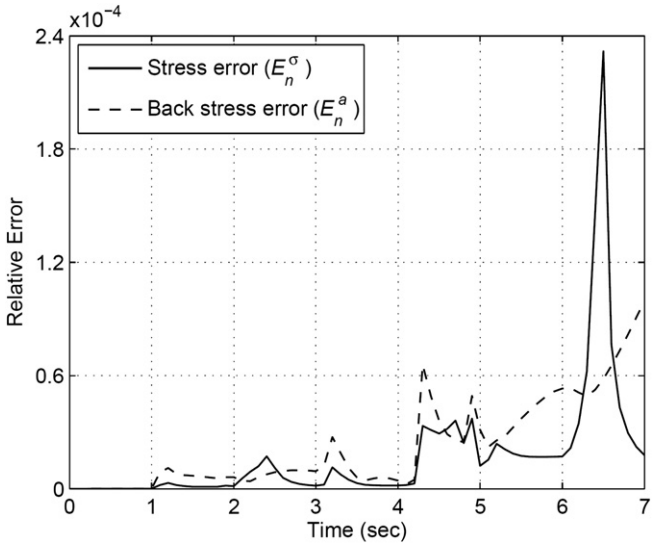

Fig. 12. Stress and back stress relative errors for history 1 by Angles-BSh32 and $Tol = 10^{-4}$.

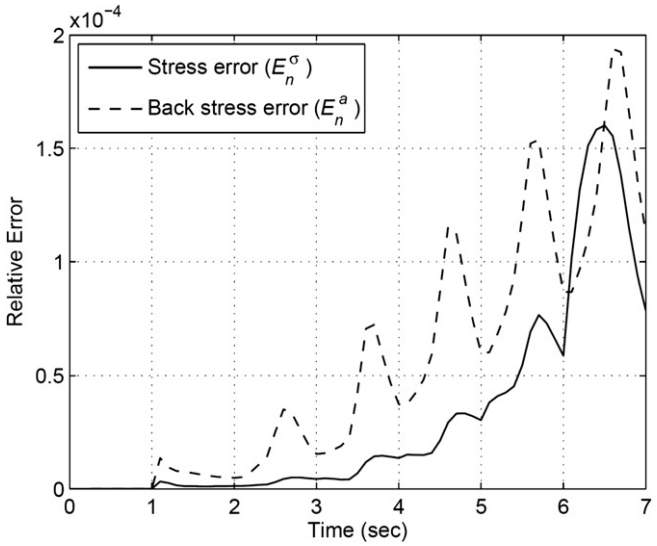

Fig. 13. Stress and back stress relative errors for history 2 by Angles-BSh32 and $Tol = 10^{-4}$.

In order to calculate error contours, it is assumed that the stress state at the time t_n is on the yield surface. Then, an arbitrary increment for the deviatoric strain $\Delta\mathbf{e}$ will be chosen to have the principal directions identical to $\mathbf{s}'_n$. To determine a strain increment $\Delta\boldsymbol{\varepsilon}$, the volumetric part of the strain must be specified. Therefore, the following parameter is used:

$$V = \frac{\Delta\varepsilon_v}{\sqrt{2}\|\Delta\mathbf{e}\|} \tag{100}$$

In this relation, V is a scalar parameter to characterize the ratio of the volumetric strain increment and the deviatoric strain increment in the load step. Now, a reference system of $(\hat{n}, \hat{t})$ is assumed as an orthogonal basis for the deviatoric plane in principal stress space. In this system, $\hat{n}$ is defined as the unit outward normal to the yield surface at $\mathbf{s}'_n$, i.e. $\hat{n} = \mathbf{s}'_n/R_n$. Subsequently, a range of the deviatoric strain increment can be produced by the parameters:

$$\begin{aligned} N &= \sqrt{2}\rho\cos\ (\psi_n) \\ T &= \sqrt{2}\rho\sin\ (\psi_n) \end{aligned} \tag{101}$$

Where,

$$\rho = \frac{2G\|\Delta\mathbf{e}\|}{R_n} \tag{102}$$

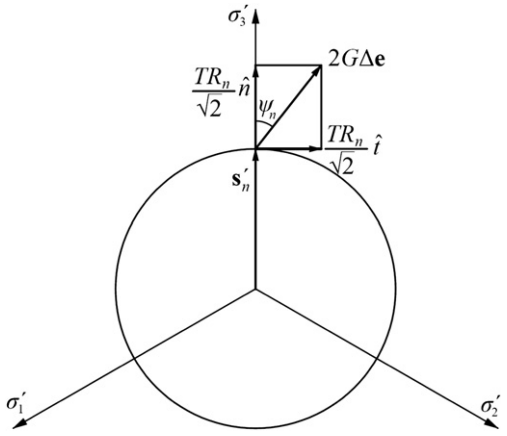

Fig. 14. Definition of the parameters T, N.

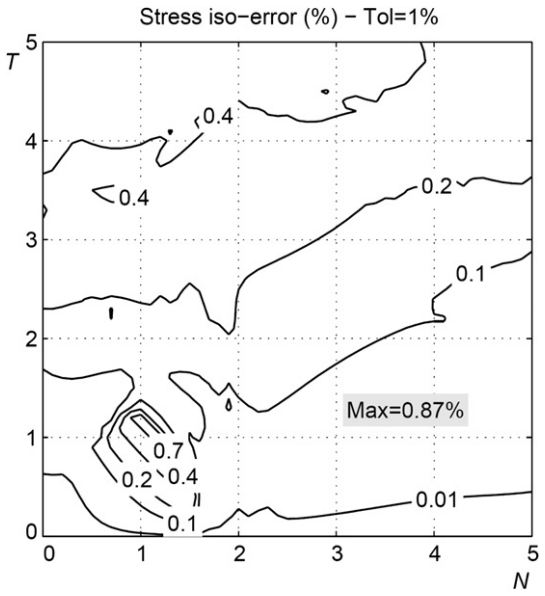

Fig. 15. Stress iso-error maps for $V = 0$.

In fact, both the direction and the amplitude pertaining to a deviatoric loading increment can be easily obtained by using these projections, N and T. The definitions of the parameters N and T are shown in Fig. 14. Finally, a unique strain increment $\Delta\boldsymbol{\varepsilon}$ is characterized by selecting values for V, N and T. To investigate the accuracy of the new integration, two different values $V = 0$ and 1 are considered and the subsequent domains of N and T for them are considered (see references: Loret and Prevost, 1986; Rezaiee-Pajand and Nasirai, 2008):

$$\begin{aligned} &0 \le N \le 5,\ \ 0 \le T \le 5 \ \text{ for } \ V = 0 \\ &-5 \le N \le 5,\ \ 0 \le T \le 5 \ \text{ for } \ V = 1 \end{aligned}$$

It should be noted that the trial stress, i.e. $2G\Delta\mathbf{e}$, lies on the deviatoric plane for $V = 0$ and the interval of ψ_n must be $[0,\ \pi/2]$ to guarantee staying in plastic phase. Therefore, the parameter N has no negative value. However, in the case of $V = 1$ the interval for ψ_n is assumed to be $[0,\ \pi]$, i.e. N can have both positive and negative values.

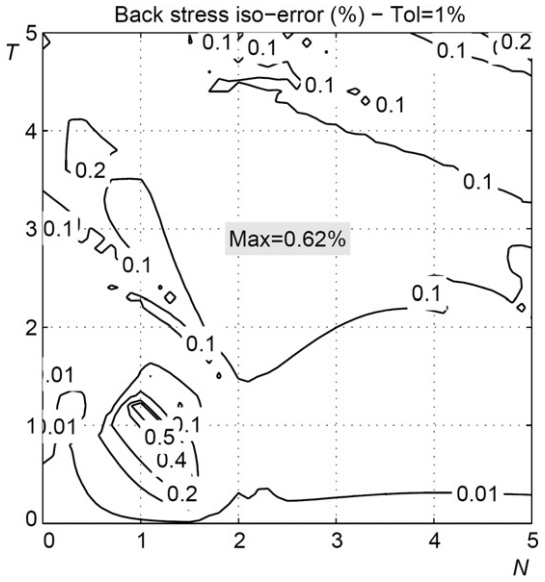

Fig. 16. Back stress iso-error maps for $V = 0$.

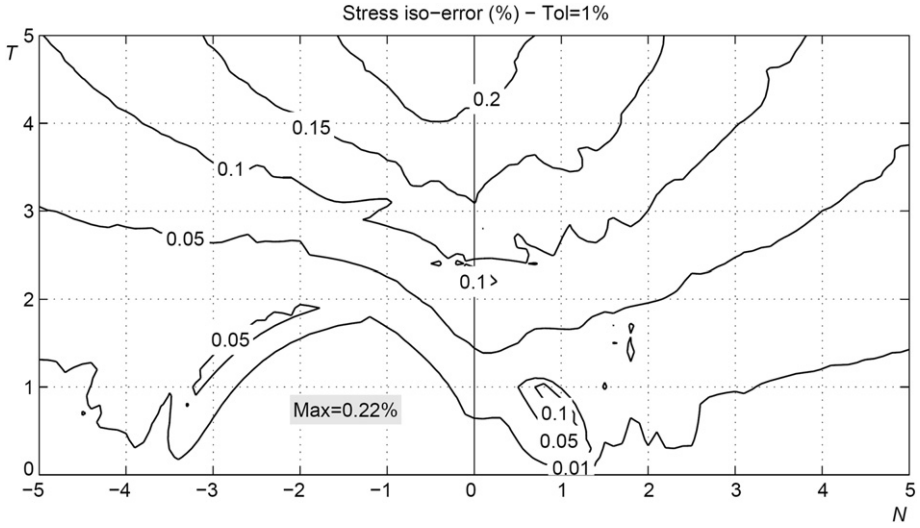

Fig. 17. Stress iso-error maps for $V = 1$.

Finally, the material state is updated by using the Angles-BSh32 with an error tolerance $Tol = 1\%$. In addition, the stresses updated by the Angles-DP54 with $Tol = 10^{-10}$ are assumed as the exact solutions. The error of updated stress and back stress are computed based on Eqs. (98) and (99). Figs. 15 and 16 show the iso-error maps for the stress and back stress in the case of $V = 0$, respectively. As it is shown, the maximum error obtained for stress and back stress are $E^{\sigma}_{\max} = 0.87\%$ and $E^{a}_{\max} = 0.62\%$, respectively, which are less than the specified error tolerance, $Tol = 1\%$. In the case of $V = 1$, the error contours are presented for updated stress and back stress in Figs. 17 and 18, respectively. The maximum values of stress error and back stress error are $E^{\sigma}_{\max} = 0.22\%$ and $E^{a}_{\max} = 0.31\%$. Therefore, for $V = 1$, the maximum errors have lower values than $Tol = 1\%$. As a result, all diagrams illustrate the robustness and accuracy of the new integration scheme.

7.3. Computation time

In this section, the efficiency and performance of the suggested integration method are tested. For this propose, computation times for the Angles-BSh32, the forward Euler and backward Euler integrations are recorded and compared. Here, it is assumed that the stress state at the time t_n lies on the yield surface, as it was explained in Section 7.2. A magnitude of deviatoric loading increment $\|\Delta\mathbf{e}\| = 1\%$ and $V = 1$ are adopted. Then, the stress state is updated with each value for ψ_n from 0 to 180° as follows:

$$\psi_n = 0,\ 0.02^{\circ},\ 0.04^{\circ},\ldots,\ 180^{\circ}$$

In fact, the stress updating of 9001 strain histories are computed with the different number of sub-steps of the strain increment to obtain the different values of errors and CPU times for each case. As a result, it is possible to compare the efficiency of the new integration scheme and Euler's integrations for a wide range of the strain steps. For each history, the total error of the updated stress is calculated by:

$$E_{\text{Total}} = \sum_{i=1}^{9001} \frac{\|\boldsymbol{\sigma}_{n+1,i} - \boldsymbol{\sigma}^{\text{E}}_{n+1,i}\|}{\|\boldsymbol{\sigma}^{\text{E}}_{n+1,i}\|} \times 100\% \tag{103}$$

Where, $\boldsymbol{\sigma}^{\text{E}}_{n+1}$ represents the updated stress computed by Angles-DP54 with $Tol = 10^{-10}$. Also, $\boldsymbol{\sigma}_{n+1}$ is the stress tensor at the time t_{n+1}, which is obtained with a different number of steps by the

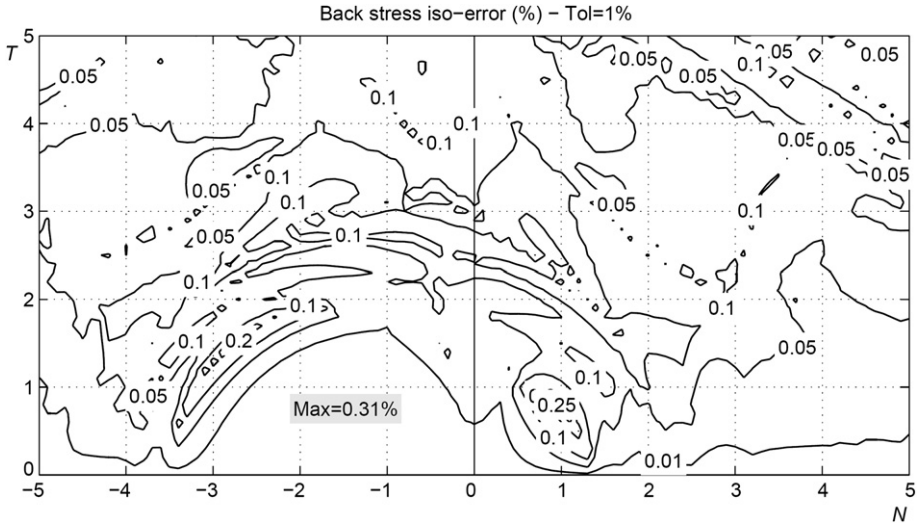

Fig. 18. Back stress iso-error maps for $V = 1$.

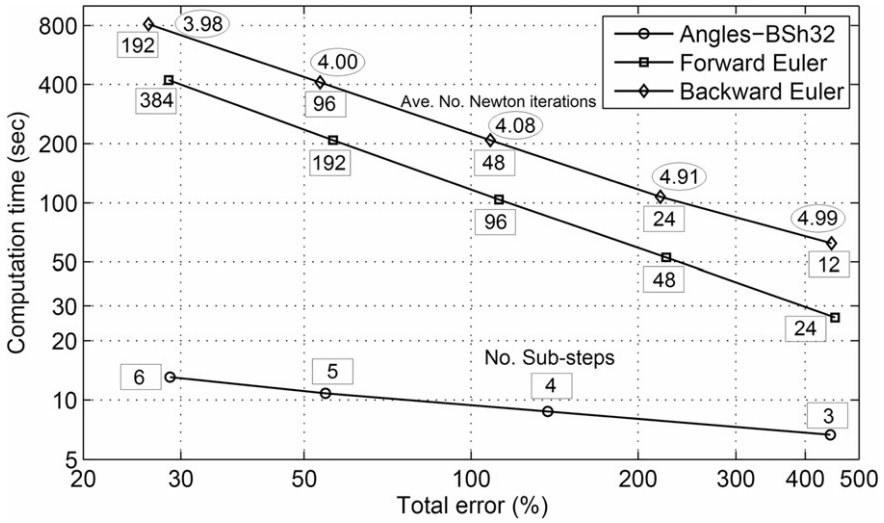

Fig. 19. Efficiency of the different stress updating algorithms in a logarithmic space.

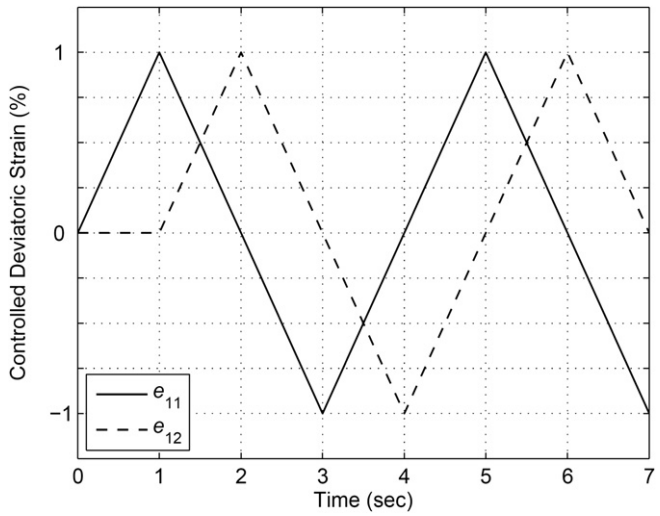

Fig. 20. Deviatoric strain history.

Angles-BSh32 method and the Euler's integrations. Fig. 19 shows the results of the computation time on a normal CPU for the Angles-BSh32, the forward Euler and backward Euler integrations versus the total error in percent. For presenting more clearly the results, the average numbers of Newton iterations per time step are given in the diagram. Also, for computing the discrete plastic multiplier, λ, an error tolerance of 10^{-12} was used. Based on these findings, the suggested integration presents the shortest CPU time, and runs for the total error $E_{\text{Total}} = 450\%$, about 4 and 9 times faster than the forward and backward Euler, respectively. In the case of high accuracy, the new scheme is very faster than the Euler's integration strategies. In other words, the efficiency of the suggested integration is not at all comparable in the high accuracies. It should be noted that reducing the constitutive equations to a few ordinary differential equations (Angles' method) and using the Bogacki-Shampine method 3(2) (BSh32) are the main reasons for obtaining to this high efficiency.

Table 1
Performances of the algorithms.

Algorithm	Max. successful sub-steps	Total successful sub-steps	Total error	CPU time (sec)
Angles-BSh32	4	57,238	49.3	15.1
Forward Euler	1	1,120,000	49.9	130.6
Backward Euler	1	448,000	46.8	224.1

An additional investigation on the efficiency and performance of the new scheme in order to clarify better is carried out. A biaxial non-proportional deviatoric strain history is considered. Other strain components are assumed to be equal to zero. This strain history is shown in Fig. 20. Moreover, the following relation defines the volumetric strain as:

$$\varepsilon_{\text{v}}(t) = 0.001\, t \tag{104}$$

It is desired to compare the computation time for updated stresses associated with this strain history by all mentioned schemes. In order to give an assessable CPU time, the strain history is repeated 200 times with a total time 1400 (sec). Furthermore, to easily evaluate the performances of all algorithms, the total error (sum of the every 0.1 (sec) stress relative errors over the total time) for all schemes are kept the same. As pervious numerical tests, the stresses computed by the Angles-DP54 with $Tol = 10^{-10}$ are considered the exact solutions. The findings are shown in Table 1. As it can be seen, the backward Euler scheme has presented the lowest performance due to its inherently iterative loops. In fact, the average number of Newton iterations per time step for backward Euler is 3.91, while the other methods do not require any iteration loops due to their explicit nature. Although the forward Euler method requires less time than the backward Euler, its CPU time is very longer than the CPU time related to the Angles-BSh32. In the other words, the new scheme is run very faster and more efficient than the forward Euler, which known as a rapid integration.

8. Conclusions

A new consistent integration formulation has been developed for the Drucker-Prager's plasticity models with Armstrong-Frederick's kinematic and linear isotropic hardenings. The suggested technique, i.e. Angles' method, is derived based on the definitions of angles between constitutive quantities. This approach reduced the constitutive equations to five ordinary differential equations that could be solved by an ODE integration procedure. The third-order Bogacki-Shampine method 3(2) (BSh32) is used for medium accuracy. Moreover, the fifth-order Dormand-Prince method 5(4) (DP54) is utilized for high accuracy. These ODE solvers have the FSAL property. Also, they can estimate the local error to

implement adaptive step size. As a result, a powerful integration with automatic error control was formulated. This strategy uses Angles' method along with the BSh32 or DP54 to update the constitutive equations. To show the accuracy and efficiency of the new scheme, a wide range of the numerical tests was presented including strain load histories, iso-error maps, and computation time. The explicit forward and implicit backward Euler integrations were also used to compare the efficiency and performance of the suggested method. These numerical studies showed the robustness and high efficiency of the new integration process. The effectiveness of the proposed approach is a result of the reduced constitutive equations and using an ODE integration technique along with error control and FSAL property.

Appendix A. Backward Euler integration

The backward Euler integration for the Drucker-Prager's plasticity model obeying the Armstrong-Frederick kinematic hardening is briefly provided. Following standard methodology, the strain rate $\dot{\boldsymbol{\varepsilon}}$ is kept constant during each load step. Therefore, a strain increment $\Delta\boldsymbol{\varepsilon} = \Delta t\dot{\boldsymbol{\varepsilon}} = \boldsymbol{\varepsilon}_{n+1} - \boldsymbol{\varepsilon}_n$ over the time interval from t_n to t_{n+1} is considered. The material state at the time t_n is known, and it is characterized by the constitutive quantities$\{\boldsymbol{\varepsilon}_n, \boldsymbol{\varepsilon}_n^{\mathrm{p}}, \boldsymbol{\sigma}_n, \mathbf{a}_n\}$. In order to integrate the constitutive equations by backward Euler scheme, an elastic predictor and a plastic corrector are used. First, the elastic predictor is assumed to be a trial solution, the same as relations have been presented in Eq. (73). Then, if the condition given in Eq. (74) is fulfilled, the trial solution is acceptable. Otherwise, a plastic corrector is needed. Now, using the return mapping algorithm, the following equations can give the deviatoric and volumetric parts of the shifted stress at the time t_{n+1}:

$$\begin{aligned}
\mathbf{s}'_{n+1} &= \frac{1}{q_1}\left(\mathbf{s}'^{\mathrm{TR}}_{n+1} + \frac{\lambda H_{\mathrm{nl}}}{1+\lambda H_{\mathrm{nl}}}\boldsymbol{\alpha}_n\right)\\
p'_{n+\alpha} &= \frac{1}{q_2}\left[p'^{\mathrm{TR}}_{n+1} + \frac{\lambda H_{\mathrm{nl}}}{1+\lambda H_{\mathrm{nl}}}\overline{p}_n + \left(\frac{2}{3}\frac{\lambda^2\beta H_{\mathrm{nl}}H_{\mathrm{kin}}}{1+\lambda H_{\mathrm{nl}}} - 2\lambda\beta\overline{K}\right)\right.\\
&\quad \left.\times(\tau_{\mathrm{y},n} + \lambda H_{\mathrm{iso}})\right]
\end{aligned} \tag{A.1}$$

Where, the scalars q_1 and q_2 are given by:

$$\begin{aligned}
q_1 &= 1 + 2\overline{G}\lambda - \frac{\lambda^2 H_{\mathrm{nl}}H_{\mathrm{kin}}}{1+\lambda H_{\mathrm{nl}}}\\
q_2 &= 1 - \lambda\overline{K}\beta^2 + \frac{2}{3}\frac{\lambda^2\beta^2 H_{\mathrm{nl}}H_{\mathrm{kin}}}{1+\lambda H_{\mathrm{nl}}}
\end{aligned} \tag{A.2}$$

The discrete plastic multiplier λ is calculated by employing the yield criterion, i.e. Eq. (1), for the material state at the time t_{n+1} as:

$$F(\mathbf{s}'_{n+1}, p'_{n+1}, \tau_{\mathrm{y},n+1}) = F(\lambda) = 0 \tag{A.3}$$

Where,

$$\tau_{\mathrm{y},n+1} = \tau_{\mathrm{y},n} + \lambda H_{\mathrm{iso}} \tag{A.4}$$

Eq (A.3) leads to a nonlinear equation that must be solved by using a numerical technique. Implementing a perturbation method, such as the Newton–Raphson iteration procedure, leads the next formula:

$$\lambda^{j+1} = \lambda^j - \frac{F\left(\lambda^j\right)}{F'\left(\lambda^j\right)} \tag{A.5}$$

Where, the superscript j denotes the jth iteration, and F' refers to the first derivative of $F(\lambda)$ with respect to λ. The iterations can be begun with $\lambda^0 = 0$ as an initial value. After converging the value of λ on a positive root, the components of the shifted stress are updated by using Eq (A.1) and (A.2). Moreover, the back stress at the end of the load step can be given by the following equations:

$$\begin{aligned}
\boldsymbol{\alpha}_{n+1} &= \frac{1}{1+\lambda H_{\mathrm{nl}}}\boldsymbol{\alpha}_n + \frac{\lambda H_{\mathrm{kin}}}{1+\lambda H_{\mathrm{nl}}}\mathbf{s}'_{n+1}\\
\overline{p}_{n+1} &= \frac{1}{1+\lambda H_{\mathrm{nl}}}\overline{p}_n + \frac{2}{3}\frac{\lambda\beta H_{\mathrm{kin}}}{1+\lambda H_{\mathrm{nl}}}(\tau_{\mathrm{y},n+1} - \beta p'_{n+1})
\end{aligned} \tag{A.6}$$

Appendix B. Forward Euler integration

To integrate the constitutive equations by explicit forward Euler scheme, the constant strain rate assumption is used. At the time t_n the constitutive quantities and the strain increment are known. First, an elastic trial solution is calculated by a relation similar to Eq. (73). Then, if the condition (74) is satisfied, the trial estimation could be admissible. If not, the load step should be divided into the elastic and plastic parts by a scalar parameteron α that has been introduced in Section 5. By using the parameter α, the deviatoric and volumetric components of the shifted stress can be determined at the contact point with the yield surface (at the time $t_{n+\alpha}$) by Eq. (77). In the next stage, the discrete plastic multiplier λ is needed to achieve the constitutive quantities at the time t_{n+1}. Using Eq. (26) and an explicit assumption, the parameter λ can be calculated as:

$$\begin{aligned}
\lambda &= \dot{\gamma}(1-\alpha)\Delta t\\
&= \frac{(1-\alpha)\left(2G\mathbf{s}'_{n+\alpha} : \Delta\mathbf{e} + \sqrt{2}\beta K\Delta\varepsilon_{\mathrm{v}}R_{n+\alpha}\right)}{2\left(\overline{G} + \overline{K}\beta^2\right)R^2_{n+\alpha} + \sqrt{2}(H_{\mathrm{iso}} - \beta H_{\mathrm{nl}}\overline{p}_n)R_{n+\alpha} - H_{\mathrm{nl}}\mathbf{s}'_{n+\alpha} : \boldsymbol{\alpha}_n}
\end{aligned} \tag{B.1}$$

Where,

$$R_{n+\alpha} = \sqrt{2}(\tau_{\mathrm{y},n} - \beta p'_{n+\alpha}) \tag{B.2}$$

Finally, the constitutive quantities can be updated by the following equations:

$$\begin{aligned}
\mathbf{s}'_{n+1} &= \mathbf{s}'_{n+\alpha} + 2G(1-\alpha)\Delta\mathbf{e} - 2\overline{G}\lambda\mathbf{s}'_{n+\alpha} + \lambda H_{\mathrm{nl}}\boldsymbol{\alpha}_n\\
\boldsymbol{\alpha}_{n+1} &= \boldsymbol{\alpha}_{n+\alpha} + \lambda H_{\mathrm{kin}}\mathbf{s}'_{n+\alpha} - \lambda H_{\mathrm{nl}}\boldsymbol{\alpha}_n\\
p'_{n+1} &= p'_{n+\alpha} + K(1-\alpha)\Delta\varepsilon_v - \sqrt{2}\beta\overline{K}\lambda R_{n+\alpha} + \lambda H_{\mathrm{nl}}\overline{p}_n\\
\overline{p}_{n+1} &= \overline{p}_n + \frac{\sqrt{2}}{3}\lambda\beta H_{\mathrm{kin}}R_{n+\alpha} - \lambda H_{\mathrm{nl}}\overline{p}_n\\
\tau_{\mathrm{y},n+1} &= \tau_{\mathrm{y},n} + \lambda H_{\mathrm{iso}}
\end{aligned} \tag{B.3}$$

Since the forward Euler integration is not consistent with the yield condition, the stress state at the end of the load step may be not located on the yield surface. Therefore, a corrector tensor should be added to the deviatoric shifted stress, $\mathbf{s}'_{n+1}$, in the normal direction to the yield surface in the deviatoric plane, i.e. $\mathbf{n}_{n+1} = \mathbf{s}'_{n+1}/\|\mathbf{s}'_{n+1}\|$. The factor of the corrector can be calculated from below relationship:

$$a_{\mathrm{f}} = \sqrt{(\mathbf{n}_{n+1} : \mathbf{s}'_{n+1})^2 - \|\mathbf{s}'_{n+1}\|^2 + R^2_{n+1}} - \mathbf{n}_{n+1} : \mathbf{s}'_{n+1} \tag{B.4}$$

References

Armstrong, P.J., Frederick, C.O., 1966. A mathematical representation of the multiaxial Bauschinger effect. Report RD/B/N731. CEGB, Central Electricity Generating Board, Berkeley, UK.

Artioli, E., Auricchio, F., Beirão da Veiga, L., 2005. Integration schemes for von-Mises plasticity models based on exponential maps: numerical investigations and theoretical considerations. Int. J. Numer. Meth. Engng 64, 1133–1165.
Artioli, E., Auricchio, F., Beirão da Veiga, L., 2006. A novel 'optimal' exponential-based integration algorithm for von-Mises plasticity with linear hardening: theoretical analysis on yield consistency, accuracy, convergence and numerical investigations. Int. J. Numer. Meth. Engng 67 (4), 449–498.
Artioli, E., Auricchio, F., Beirão da Veiga, L., 2007. Second-order accurate integration algorithms for von-Mises plasticity with a nonlinear kinematic hardening mechanism. Comput. Methods Appl. Mech. Engrg 196, 1827–1846.
Auricchio, F., Beirão da Veiga, L., 2003. On a new integration scheme for von-Mises plasticity with linear hardening. Int. J. Numer. Meth. Engng 56, 1375–1396.
Bogacki, P., Shampine, L.F., 1989. A 3(2) pair of Runge–Kutta formulas. Appl. Math. Lett. 2 (4), 321–325.
Clausen, J., Damkilde, L., Anderson, L., 2006. Efficient return algorithms for associated plasticity with multiple yield planes. Int. J. Numer. Meth. Engng 66, 1036–1059.
Coombs, W.M., Crouch, R.S., Augarde, C.E., 2010. Reuleaux plasticity: analytical backward Euler stress integration and consistent tangent. Comput. Methods Appl. Mech. Engrg 199, 1733–1743.
de Souza Neto, E.A., Perić, D., Owen, D.R.J., 2008. Computational methods for plasticity: Theory and applications. John Wiley and Sons, Ltd.
Dodds, R.H., 1987. Numerical techniques for plasticity computations in finite element analysis. Comput. Structures 26 (5), 767–779.
Dormand, J.R., Prince, P.J., 1980. A family of embedded Runge-Kutta formulae. J. Comp. Appl. Math. 6 (1), 19–26.
Drucker, D.C., Prager, W., 1952. Soil mechanics and plastic analysis or limit design. Quart. Appl. Math. 10, 157–165.
Ellsiepen, P., Hartmann, S., 2001. Remarks on the interpretation of current non-linear finite element analyses as differential-algebraic equations. Int. J. Numer. Meth. Engng 51, 679–707.
Genna, F., Pandolfi, A., 1994. Accurate numerical integration of Drucker-Prager's constitutive equations. Meccanica 29, 239–260.
Hartmann, S., 2005. A remark on the application of the Newton-Raphson method in non-linear finite element analysis. Comput. Mech. 36, 100–116.
Hong, H.-K., Liu, C.-S., 2000. Internal symmetry in the constitutive model of perfect elasto-plasticity. Int. J. Non-Linear Mech. 35, 447–466.
Hong, H.-K., Liu, C.-S., 2001. Lorentz group on Minkowski spacetime for construction of the two basic principles of plasticity. Int. J. Non-Linear Mech. 36, 679–686.
Hopperstad, O.S., Remseth, S., 1995. A return mapping algorithm for a class of cyclic plasticity models. Int. J. Numer. Meth. Engng 38, 549–564.
Kobayashi, M., Ohno, N., 2002. Implementation of cyclic plasticity models based on a general form of kinematic hardening. Int. J. Numer. Meth. Engng 53, 2217–2238.
Kobayashi, M., Mukai, M., Takahashi, H., Ohno, N., Kawakami, T., Ishikawa, T., 2003. Implicit integration and consistent tangent modulus of a time-dependent non-unified constitutive model. Int. J. Numer. Meth. Engng 58, 1523–1543.
Kossa, A., Szabó, L., 2009. Exact integration of the von Mises elastoplasticity model with combined linear isotropic-kinematic hardening. Int. J. Plasticity 25, 1083–1106.
Krieg, R.D., Krieg, D.B., 1977. Accuracies of numerical solution methods for the elastic-perfectly plastic model. J. Pressure Vessel Technol. Transaction ASME 99, 510–515.
Lei, X., Lissenden, C.J., 2007. Pressure sensitive nonassocaitive plasticity model for DRA composites. J. Eng. Mater. Technol. ASME 129, 255–264.
Liu, C.-S., 2003. Symmetry groups and the pseudo-Riemann spacetimes for mixed-hardening elasto-plasticity. Int. J. Solids Struct. 40, 251–269.
Liu, C.-S., 2004a. A consistent numerical scheme for the von-Mises mixed-hardening constitutive equations. Int. J. Plasticity 20, 663–704.
Liu, C.S., 2004b. Internal Symmetry groups for the Drucker-Prager material model of plasticity and numerical integrating methods. Int. J. Solids Struct. 41, 3771–3791.
Loret, B., Prevost, J.H., 1986. Accurate numerical solutions for Drucker-Prager elastic-plastic models. Comput. Methods Appl. Mech. Engrg 54, 259–277.
Ortiz, M., Popov, E.P., 1985. Accuracy and stability of integration algorithms for elasto-plastic constitutive relations. Int. J. Numer. Meth. Engng 21, 1561–1576.
Ortiz, M., Simo, J.C., 1896. An analysis of a new class of integration algorithms for elasto-plastic constitutive relations. Int. J. Numer. Meth. Engng 23, 353–366.
Rezaiee-Pajand, M., Nasirai, C., 2007. Accurate integration scheme for von-Mises plasticity with mixed-hardening based on exponential maps. Eng. Computations 24 (6), 608–635.
Rezaiee-Pajand, M., Nasirai, C., 2008. On the integration schemes for Drucker-Prager's elasto-plastic models based on exponential maps. Int. J. Numer. Meth. Engng 74, 799–826.
Rezaiee-Pajand, M., Nasirai, C., Sharifian, M., 2010. Application of exponential-based methods in integrating the constitutive equations with multicomponent kinematic hardening. J. Eng. Mech. ASCE 136 (12), 1502–1518.
Rezaiee-Pajand, M., Sharifian, M., Sharifian, M., 2011. Accurate and approximate integrations of Drucker-Prager Plasticity with linear isotropic and kinematic hardening. Eur. J. Mechanics A/Solids 30, 345–361.
Ristinmaa, M., Tryding, J., 1993. Exact integration of constitutive equations in elasto-plasticity. Int. J. Numer. Meth. Engng 36, 2525–2544.
Runesson, K., Sture, S., Willam, K., 1988. Integration in computational plasticity. Comput. Structures 30 (1/2), 119–130.
Shampine, L.F., Watts, H.A., 1976. Global error estimation for ordinary differential equations. ACM Trans. Math. Software 2 (2), 172–186.
Simo, J.C., Taylor, R.L., 1986. A return mapping algorithm for plane stress elasto-plasticity. Int. J. Numer. Meth. Engng 22, 649–670.
Simo, J.C., Hughes, T.J.R., 1998. Computational inelasticity. Springer-Verlag, New York.
Sloan, S.W., Booker, J.R., 1992. Integration of Tresca and Mohr-Coulomb constitutive relations in plane strain elasto-plasticity. Int. J. Numer. Meth. Engng 33, 163–196.
Sloan, S.W., Abbo, A.J., Sheng, D., 2001. Refined explicit integration of elasto-plastic models with automatic error control. Eng. Computations 18 (1/2), 121–154.
Spitzig, W.A., Richmond, O., 1984. The effect of pressure on the flow stress metals. Acta Metal 32 (3), 457–463.
Szabó, L., 2009. A semi-analytical integration method for J2 flow theory of plasticity with linear isotropic hardening. Comput. Methods Appl. Mech. Engrg 198, 2151–2166.
Wallin, M., Ristinmaa, M., 2001. Accurate stress updating algorithm based on constant strain rate assumption. Comput. Methods Appl. Mech. Engrg 190, 5583–5601.
Wallin, M., Ristinmaa, M., 2008. An alternative method for the integration of continuum damage evolution laws. Comput. Mech. 41, 347–359.
Wei, Z., Perić, D., Owen, D.R.J., 1996. Consistent linearization for the exact stress update of Prandtl-Reuss non-hardening elasto-plastic models. Int. J. Numer. Meth. Engng 39, 1219–1235.
Wilkins, M.L., 1964. Calculation of Elastic-plastic Flow. Method of Computational Physics, vol. 3. Academic Press.
Yoder, P.J., Whirley, R.G., 1984. On the numerical implementation of elasto-plastic models. J. Appl. Mech. ASME 51, 283–288.